SIAM J. SCI. COMPUT.
Vol. 36, No. 3, pp. B561–B588

ANALYSIS OF THE TWO-REGIME METHOD ON SQUARE MESHES*

MARK B. FLEGG†, S. JONATHAN CHAPMAN†, LIKUN ZHENG‡, AND RADEK ERBAN†

Abstract. The two-regime method (TRM) has been recently developed for optimizing stochastic reaction-diffusion simulations [M. Flegg, J. Chapman, and R. Erban, *J. Roy. Soc. Interface*, 9 (2012), pp. 859–868]. It is a multiscale (hybrid) algorithm which uses stochastic reaction-diffusion models with different levels of detail in different parts of the computational domain. The coupling condition on the interface between different modeling regimes of the TRM was previously derived for one-dimensional models. In this paper, the TRM is generalized to higher dimensional reaction-diffusion systems. Coupling Brownian dynamics models with compartment-based models on regular (square) two-dimensional lattices is studied in detail. In this case, the interface between different modeling regimes contains either flat parts or right-angle corners. Both cases are studied in the paper. For flat interfaces, it is shown that the one-dimensional theory can be used along the line perpendicular to the TRM interface. In the direction tangential to the interface, two choices of the TRM parameters are presented. Their applicability depends on the compartment size and the time step used in the molecular-based regime. The two-dimensional generalization of the TRM is also discussed in the case of corners.

Key words. stochastic reaction-diffusion simulations, two-regime method, multiscale modeling

AMS subject classifications. 92C40, 82C31, 60G50, 80A30

DOI. 10.1137/130915844

1. Introduction.

There are two common approaches to stochastic reaction-diffusion modeling: (i) compartment-based models and (ii) molecular-based models [7, 6]. Molecular-based models provide a higher level of detail, but they are often more computationally intensive than compartment-based models. In some applications, microscopic detail are only required in a relatively small region, for example, close to the cellular membrane or a particular organelle [11, 8]. Such problems may be best simulated by a hybrid method which uses a detailed modeling approach in localized regions of particular interest (in which accuracy and microscopic detail are important) and a less detailed model in other regions in which accuracy may be traded for simulation efficiency. A variety of such hybrid methods have been proposed in recent years. Some of these algorithms aim to couple mesoscopic stochastic simulations on a lattice with a deterministic PDE-based mean-field description [1, 12, 33, 26]. Others provide a way to couple deterministic PDE-based descriptions with microscopic molecular-based simulations [14, 18, 13]. Algorithms which provide a way to couple mesoscopic compartment-based and microscopic molecular-based approaches have also been published [23, 20, 10].

*Submitted to the journal's Computational Methods in Science and Engineering section April 5, 2013; accepted for publication (in revised form) March 4, 2014; published electronically June 17, 2014. This work was supported by the *European Research Council* under the *European Community's* Seventh Framework Programme (*FP7/2007-2013*)/ ERC grant agreement No. 239870 and in part by Award No. KUK-C1-013-04 made by King Abdullah University of Science and Technology (KAUST).
http://www.siam.org/journals/sisc/36-3/91584.html

†Mathematical Institute, University of Oxford, Radcliffe Observatory Quarter, Woodstock Road, Oxford OX2 6GG, United Kingdom (mark.flegg@monash.edu, chapman@maths.ox.ac.uk, erban@maths.ox.ac.uk). The fourth author's work was also supported by a Royal Society University Research Fellowship; by a Nicholas Kurti Junior Fellowship from Brasenose College, University of Oxford; and by the Philip Leverhulme Prize from the Leverhulme Trust.

‡Department of Mathematics, University of California, Irvine, Irvine, CA 92697 (likunz@uci.edu).

Algorithms which couple mesoscopic stochastic simulations on a lattice with a deterministic PDE-based mean-field description [1, 12, 33, 26] typically do not separate PDE and lattice regions cleanly but rather include the use of an overlap region. In this overlap the flux of molecules (and other conserved physical quantities) flowing between the two regimes is matched. The flux is first calculated by particle counting and then imposed as a boundary condition on the PDE [1, 12, 33, 26]. New particles are created either in the compartment closest to the interface [12, 33] or in a pseudo-compartment corresponding to the first grid point of the PDE solver ("handshaking region") [1].

Ferm, Hellander, and Lötstedt [9] presented a new technique for connecting deterministic regions with mesoscopic regions using a smoother coupling technique. Their technique involves interfacing a region of deterministic description with a stochastic description modeled using a tau leaping algorithm [17]. This stochastic simulation technique is fast but is accurate only if the concentration of molecules is large enough that individual events on smaller time scales produce small perturbations that do not affect the simulation significantly. This tau leaping algorithm is then interfaced with a more accurate compartment-based algorithm as the concentration drops.

Geyer and others [14, 18] developed a method for coupling a deterministic numerical solution to a reaction-diffusion PDE with a Brownian dynamics molecular-based algorithm. In a similar way to the previous algorithms which couple deterministic PDEs and compartment-based algorithms, the flux is determined at the interface. Molecules are initiated in the molecular-based algorithm in one dimension using the same distribution which is also applied later in this manuscript for coupling compartment-based and molecular-based models (1.12) (see (11) in [14]).

The matching condition used to transition between two separate modeling regimes usually has two features which can cause complications. First, when coupling a deterministic PDE model with a stochastic one such as a compartment-based or molecular-based model, the boundary condition for the PDE model at the interface is often dictated by an averaging of particle flux from the stochastic simulation. This is fine if the stochastic region has a large flux, but if this flux is small (which justifies the use of the stochastic model in the first place), then the flux consists of sporadic individual molecules which are not treated stochastically at the interface. Second, coupling is usually done with the use of overlap regions which gradually transition between the modeling regimes. Defining an overlap region can offer accurate results but introduces new problems, such as the treatment of reacting molecules in the overlap region. Overlap regions also require significant and purposeful recoding of existing modeling algorithms.

Franz et al. [13] recently developed a technique for coupling deterministic PDEs with microscopic molecular-based simulations. This method does not use an averaging technique to determine the flux over the interface but treats each particle/molecule as an individual as it crosses from the molecular-based simulation. The continuous distribution of particles on the PDE side is interpreted as a probability density, and each new particle adds to this probability distribution as it crosses. Conversely, molecules may migrate back with a probability determined from the continuous distribution as it leeches back onto the discrete side. As with other methods, it was found that the introduction of an overlap region produced more accurate results.

While it has been shown that errors generated by transition between multiscale regimes can be reduced by increasing the size of the zone of "overlap," the existence of these regions raises questions about the correct implementation of

molecular interaction/reaction and introduces a new complexity to the algorithms. In order to transition molecules between two distinct multiscale regions, the molecules must be treated very carefully on the boundary to minimize the possible error.

In a paper in 2012 we presented the appropriate boundary condition for coupling one-dimensional (1D) compartment-based and molecular-based models in the absence of an overlap region [10]. The two-regime method (TRM) has the accuracy of the detailed molecular-based approach (in the region where it is required), but benefits from the efficiency of a less detailed (coarser) compartment-based model in other parts of the computational domain. The TRM, importantly, treats each molecule individually at the interface. This is because both regimes in the TRM are stochastic (often containing low copy numbers) and the trajectories of discrete numbers of molecules are, in some sense, traced in both regimes. The TRM is implemented in a similar way to the algorithms found in [23, 20], but it uses careful transition rules which minimize the error that is generated by the interface. The lack of an overlap region for the TRM significantly simplifies its implementation, but it is important to understand the sources of error to determine when a more complex overlapping technique should be used.

As computational biology progresses and greater demands are placed on computational models to simulate increasingly complex systems which span different scales, coupling methods such as the TRM and other hybrid approaches [20] will become crucial tools. The TRM has previously been used to investigate the stochastic kinetics of calcium puffs from the endoplasmic reticulum [11] and the growth of filopodia by the polymerization of actin monomers [8].

In the remainder of this introductory section, we introduce the notation which is used in the rest of this manuscript. We summarize both compartment-based (section 1.1) and molecular-based modeling (section 1.2) with sufficient detail to analyze the TRM in context. Then we introduce the TRM in section 1.3. Our main results are presented and derived in section 2. In section 3, we demonstrate the applicability of the theory using several illustrative numerical examples. Finally in section 4, we investigate ways to minimize numerical artifacts and discuss the alternative algorithms by Klann, Ganguly, and Koeppl [23] and Hellander, Hellander, and Lötstedt [20].

1.1. Compartment-based modeling. Mesoscale compartment-based modeling of reaction-diffusion processes begins by partitioning the domain Ω_C into compartments (open sets) $\mathcal{C}_j$, $j = 1, \ldots, K$, such that the compartments do not overlap and they cover the whole domain Ω_C (i.e., $\cup_{j=1}^{K} \overline{\mathcal{C}}_j = \overline{\Omega_C}$ and $\mathcal{C}_i \cap \mathcal{C}_j = \emptyset$ for $i \neq j$, where overbars denote the closure of the corresponding set). Assuming that there are M chemical species $\mathcal{Z}_i$, $i = 1, \ldots, M$, the state of the system is completely defined by the copy numbers $\mathcal{N}_{i,j} \in \mathbb{N}_0$ of molecules for chemical species $\mathcal{Z}_i$ found in the compartment $\mathcal{C}_j$, $i = 1, \ldots, M$, $j = 1, \ldots, K$. In what follows, symbol $\mathbb{N}_0$ denotes the set of nonnegative integers, i.e., $\mathbb{N}_0 \equiv \{0, 1, 2, 3, \ldots\}$. The simulation of reaction and diffusion of molecules in the system is usually implemented by event-driven algorithms, which include the Gillespie algorithm [16], the Next Reaction Method [15], or the next subvolume method [19]. They have been implemented in several open-source software packages including MesoRD [19], URDME [4], STEPS [34], and SmartCell [2]. In this paper, we will use a derivative of the next reaction method from Gibson and Bruck [15]. In the literature, a compartment-based approach has a number of different names, including on-lattice, mesoscopic, and position-jump modeling. Note also that the term "compartment-based model" is occasionally used to refer to coarser, lumped-parameter models in which a small number of spatially uniform,

well-mixed regions are considered (e.g., cell cytoplasm and nucleus as two compartments). Compartment-based models, in the context of this manuscript, will refer to models in which the domain is artificially decomposed into well-mixed compartments (sometimes called voxels) at a given level of spatial resolution.

Event-driven algorithms require the calculation of event propensities for a particular system state [16]. An event propensity $\alpha_{\mathcal{E}}$ is the rate (per unit time) for an event $\mathcal{E}$ to occur that changes the state of the system. Events in compartment-based reaction-diffusion processes may include reaction events (in which chemical molecules of some species change into molecules of other species, or are just introduced or removed from the system), diffusive events (in which molecules of a chemical species jump from one compartment to an adjacent compartment), or boundary events (in which molecules are absorbed by, react with, or reflect from a domain boundary). A putative time $t_{\mathcal{E}}$ for each event $\mathcal{E}$ can be found given some current time t using

$$t_{\mathcal{E}} = t + \frac{1}{\alpha_{\mathcal{E}}} \ln\left(\frac{1}{r_{\mathcal{E}}}\right), \tag{1.1}$$

where $r_{\mathcal{E}}$ are uniformly distributed random numbers between 0 and 1 chosen separately for each occurence of each event. The next event which takes place in the system is determined by finding which event corresponds to time $\min_{\mathcal{E}} t_{\mathcal{E}}$ where the minimum is taken over the set of all possible events [15]. The state is changed to reflect the occurence of the event and the current time is then updated to $t := \min_{\mathcal{E}} t_{\mathcal{E}}$. The current event might also change propensities of some related events. The putative times for these events must therefore be scaled to reflect the change in propensity. That is,

$$t_{\mathcal{E}}^{\text{new}} := t + \frac{\alpha_{\mathcal{E}}^{\text{old}}}{\alpha_{\mathcal{E}}^{\text{new}}} \left(t_{\mathcal{E}}^{\text{old}} - t\right), \tag{1.2}$$

where $\alpha_{\mathcal{E}}^{\text{old}}$ and $\alpha_{\mathcal{E}}^{\text{new}}$ (resp., $t_{\mathcal{E}}^{\text{old}}$ and $t_{\mathcal{E}}^{\text{new}}$) are the propensities (resp., putative times) for event $\mathcal{E}$ before and after the current event takes place [15]. A putative time for the next occurence of the current event must be resampled using formula (1.1). The simulation is then constructed by a series of successive events over time, in each instance, defined by the most imminent event and performing the state change that defines that event.

1.1.1. Reaction events. One of the main assumptions of compartment-based modeling of stochastic reaction-diffusion models is that each compartment is small enough that it may be considered well mixed [31, 7]. Reactions are modeled in each compartment by defining the propensity for reaction in each compartment. Consider the reaction $\mathcal{R}$ in compartment $\mathcal{C}_j$ given by the general form

$$\sum_{i=1}^{M} \beta_i \mathcal{Z}_i \xrightarrow{\kappa} \sum_{i=1}^{M} \gamma_i \mathcal{Z}_i, \tag{1.3}$$

where $\beta_i \in \mathbb{N}_0$ (resp., $\gamma_i \in \mathbb{N}_0$) are the numbers of molecules of chemical $\mathcal{Z}_i$, $i = 1, 2, \ldots, M$, that are required as reactants (resp., products) of the chemical reaction $\mathcal{R}$ and κ is the reaction rate for one possible combination of reactants.[1] We define

[1] κ is equal to the standard (macroscopic) reaction rate if $\beta_i \leq 1\ \forall i$. Otherwise, it differs by a combinatorial factor which considers the number of ways of labeling identical reactants [16].

TABLE 1

Examples of propensities and effects of reactions in compartments. To simplify this table, we omit species with zero coefficients in reaction and product complexes which were included in the general form (1.3).

Example reaction $\mathcal{R}$	$\alpha_{\mathcal{R},j}$	Changes of the state vector
$\mathcal{Z}_i + \mathcal{Z}_k \xrightarrow{\kappa} \mathcal{Z}_l$	$\dfrac{\kappa \mathcal{N}_{i,j}\mathcal{N}_{k,j}}{V_j}$	$\mathcal{N}_{i,j}$ changes to $\mathcal{N}_{i,j}-1$ $\mathcal{N}_{k,j}$ changes to $\mathcal{N}_{k,j}-1$ $\mathcal{N}_{l,j}$ changes to $\mathcal{N}_{l,j}+1$
$2\mathcal{Z}_i \xrightarrow{\kappa} \mathcal{Z}_l$	$\dfrac{\kappa \mathcal{N}_{i,j}(\mathcal{N}_{i,j}-1)}{2V_j}$	$\mathcal{N}_{i,j}$ changes to $\mathcal{N}_{i,j}-2$ $\mathcal{N}_{l,j}$ changes to $\mathcal{N}_{l,j}+1$
$\mathcal{Z}_i \xrightarrow{\kappa} \mathcal{Z}_k + \mathcal{Z}_l$	$\kappa \mathcal{N}_{i,j}$	$\mathcal{N}_{i,j}$ changes to $\mathcal{N}_{i,j}-1$ $\mathcal{N}_{k,j}$ changes to $\mathcal{N}_{k,j}+1$ $\mathcal{N}_{l,j}$ changes to $\mathcal{N}_{l,j}+1$
$\emptyset \xrightarrow{\kappa} \mathcal{Z}_l$	κV_j	$\mathcal{N}_{l,j}$ changes to $\mathcal{N}_{l,j}+1$

the notation for this event $\mathcal{E} = (\mathcal{R}, j)$. In realizing this reaction event in the jth compartment, the number of molecules $\mathcal{N}_{i,j}$, $i = 1, 2, \ldots, M$, $j = 1, 2, \ldots, K$, change by the corresponding stoichiometric coefficient $\nu_i = \gamma_i - \beta_i$. Considering mass action chemical kinetics, the propensity for this event to occur depends on the number of available reactants in the compartment $\mathcal{C}_j$. In three dimensions, we can postulate this dependence in the following form [6, 7]:

$$\alpha_{\mathcal{R},j} = \kappa V_j^{1-\sum_i \beta_i} \prod_{i=1}^{M} \binom{\mathcal{N}_{i,j}}{\beta_i}, \tag{1.4}$$

where $(\cdot)$ represents a binomial coefficient and V_j is the volume of the compartment $\mathcal{C}_j$. Table 1 shows examples of propensity $\alpha_{\mathcal{R},j}$ for some simple reactions $\mathcal{R}$ in compartment $\mathcal{C}_j$ and the subsequent changes to the state of the system that occur as a result of the reaction event.

The main focus of this paper is on two-dimensional (2D) simulations. In this case, formula (1.4) has to be slightly modified by replacing the compartment volume V_j by its area. Since the propensity $\alpha_{\mathcal{R},j}$ is dimensionless, some rate constants have different physical units in two dimensions than in three dimensions. In applications, 2D simulations in the domain $\Omega_C \subset \mathbb{R}^2$ are often viewed as a model of a real three-dimensional (3D) domain $\Omega_C \times (0, w)$, where the domain width w is so small that the spatial distribution along the third axis can be neglected. Then formula (1.4) can be applied with the standard interpretation (i.e., physical units) of the reaction rates. The area of each 2D compartment is multiplied by w to get the corresponding volume V_j in (1.4).

1.1.2. Diffusion events. Diffusion in compartment-based models of reaction-diffusion processes is defined by the stochastic jumping of molecules of chemical species $\mathcal{Z}_i$, $i = 1, 2, \ldots, M$, between any two adjacent compartments from $\mathcal{C}_j$ to $\mathcal{C}_k$, $j, k = 1, 2, \ldots, K$. We shall define the notation for this diffusive event to be $\mathcal{E} = (\mathcal{D}, i, j, k)$. The propensity for a diffusive event is given by

$$\alpha_{\mathcal{D},i,j,k} = q_{j,k} D_i \mathcal{N}_{i,j}, \tag{1.5}$$

where $q_{j,k}$ is dependent on the morphology and relative positions of the compartments $\mathcal{C}_j$ and $\mathcal{C}_k$, and D_i is the diffusion constant for chemical $\mathcal{Z}_i$. For adjacent square or cubic compartments $\mathcal{C}_j$ and $\mathcal{C}_k$ of length h on a regular lattice, we have $q_{j,k} = 1/h^2$, i.e.,

$$\alpha_{\mathcal{D},i,j,k} = \frac{D_i}{h^2}\mathcal{N}_{i,j}, \tag{1.6}$$

and $q_{j,k} = 0$ if $\mathcal{C}_j$ and $\mathcal{C}_k$ do not share a common side. For more irregular compartment shapes, $q_{j,k}$ can be determined by the finite element discretization of the diffusion equation on a lattice whose vertices are at the centers of the compartments [4]. During the diffusive event $(\mathcal{D}, i, j, k)$, the state of the system is changed to reflect the movement of one molecule of $\mathcal{Z}_i$ from $\mathcal{C}_j$ to $\mathcal{C}_k$, i.e., $\mathcal{N}_{i,j}$ changes to $\mathcal{N}_{i,j} - 1$ and $\mathcal{N}_{i,k}$ changes to $\mathcal{N}_{i,k} + 1$.

Since we will talk later about the limit $h \to 0$ in compartment-based models it is worth mentioning here that there is a practical lower limit on h if bimolecular reactions are to be modeled correctly (comparable in size to the reaction radius in section 1.2.1) [5]. If the compartments are too small, molecules do not encounter each other freqently enough to react at the required rate even if the intracompartmental reaction rate is increased. One mechanism for avoiding this lack of convergence is to allow molecules in different compartments to react, as in [21], but this introduces more complexity into the algorithm.

1.1.3. Boundary events. Boundary events are caused by the diffusion of molecules into the boundaries of the domain $\partial\Omega_C$. It is no surprise then that boundary events are linked closely to diffusion events. Consider the compartment $\mathcal{C}_j$ which is adjacent to $\partial\Omega_C$. A diffusive event of a molecule of chemical $\mathcal{Z}_i$ which would ordinarily result in a jump from $\mathcal{C}_j$ to a compartment on the other side of $\partial\Omega_C$ actually results in an interaction of the molecule with the boundary. Such an interaction usually results in one of two outcomes: either the molecule is absorbed or the molecule is reflected with some probability dependent on the particular boundary condition. This probability can be related to the deterministic reactivity constant K [5]. Reversible boundary reactions can be modeled by including a surface concentration of molecules [20]. The TRM involves the use of a pseudoboundary, shared by both molecular-based and compartment-based modeling approaches (which we label as the interface). It can be shown that this interface corresponds, for molecules on both sides, to a boundary with reactivity $K \to \infty$ [5, 10]. For all other boundaries in this paper we will use reflective boundary conditions.

1.2. Molecular-based modeling. Molecular-based approaches to reaction-diffusion modeling are characterized by the prescription of exact coordinates in space for each molecule of each chemical species $\mathcal{Z}_i$, $i = 1, 2, \ldots, M$, in the continuous domain $\Omega_M \subset \mathbb{R}^N$, where $N = 1, 2, 3$. The trajectory of large molecules (such as proteins) are computed using Brownian dynamics [3, 13, 30]. Molecular-based models have been implemented in several software packages, including Smoldyn [3], MCell [28], and Green's function reaction dynamics (GFRD) [32]. They have been used for modeling several biological systems, including the signal transduction in bacterium *E. coli* [25] and the MAPK pathway [29].

There are many different ways that molecular-based simulations are implemented. The most basic type of simulation is a time-driven approach [3]. The strength of this approach is its simplicity, which allows for hassle-free coding but at the cost of computational time. It involves updating the positions of all molecules using a

continuous-space random walk and then comparing the relative positions of reactants for possible reactions.

Other schemes for molecular-based simulation of reaction-diffusion processes can generally be related to the GFRD paradigm [32] or the variants of the first passage kinetic Monte Carlo (FPKMC) method [27, 29]. GFRD updates time according to an adaptive time step scheme. The time step at any moment in the algorithm is calculated such that it is highly unlikely that for any particular molecule a bimolecular reaction could occur with any more than one other specific molecule, but otherwise the time step is maximized. In this way, temporal instances of relative high molecular sparcity will allow the algorithm to progress quickly. It also means that reactions can be analytically solved for under the assumption that between two moments in time the system is a set of distinct one-molecule and two-molecule systems. The FPKMC paradigm describes each molecule as contained in a sphere. The time to exit the sphere is sampled for each molecule, and when molecules are close enough together they are considered as a two-molecule system in a new sphere. None of the spheres overlap and precise first passage times (for exiting molecules or reacting molecules) are sampled for each sphere. The algorithm progresses by asynchronous updates of the exit and reaction events, and at each time, new encapsulating spheres are generated for each molecule (or pair of reacting molecules).

The accuracy of the GFRD paradigm rests on the assumption that the system can be broken into disjoint one- and two-molecule systems. The accuracy of the FPKMC paradigm variants can be reduced to how accurate the sampling of exit times can be from their analytical distributions. The FPKMC has the added advantage over the GFRD that it allows effectively for large time steps in spatial regions of high sparcity (with larger, nonoverlapping spheres) while the GFRD forces every molecule to undergo updates depending on the clustering of the closest three molecules in the system.

The coupling condition at the interface for the TRM is conditional on the time step parameter Δt and therefore we will demonstrate how molecules behave in a time-driven regime. Note that if the molecule-based domain is governed by a GFRD algorithm, then the interface coupling should match the current value of Δt within the algorithm, and if an FPKMC equivalent method is being used, then a finite Δt needs to be prescribed to update molecules at the interface (but in such a case, the Δt can be specifically chosen to minimize the error, as we shall see).

A molecule in a time-driven molecular-based algorithm is treated as follows. The effect of solvent molecules on the large molecules of interest are modelled by generating a random displacement in the large molecules every timestep Δt. Modelling the large molecules in this way allows us to ignore the simulation of individual solvent molecules. We will denote the jth molecule of chemical species $\mathcal{Z}_i$ as Z_i^j. Given a time step Δt the position $\mathbf{x}_{i,j}(t + \Delta t)$ of molecule Z_i^j at time $t + \Delta t$ is computed from its position $\mathbf{x}_{i,j}(t)$ at time t in the N-dimensional continous space Ω_M by

$$\mathbf{x}_{i,j}(t + \Delta t) = \mathbf{x}_{i,j}(t) + \sqrt{2D_i \Delta t}\, \boldsymbol{\zeta}, \tag{1.7}$$

where $\boldsymbol{\zeta} \in \mathbb{R}^N$ is a vector of N uncorrelated normally distributed random numbers with zero mean and unit variance chosen separately for each molecule. Equation (1.7) is a discretization of the standard Brownian motion

$$\mathrm{d}\mathbf{X}_{i,j} = \sqrt{2D_i}\, \mathrm{d}\mathbf{W}_{\mathbf{i,j}}, \tag{1.8}$$

where $\mathbf{W}_{\mathbf{i,j}}$ denotes N independent Wiener processes for each set of indicies.

1.2.1. Chemical reactions. It is relatively straightforward to implement zero-order and first-order chemical reactions in molecular-based models [7]. There are a variety of ways to model bimolecular (second-order) molecular-based reactions. Consider two molecules Z_i^j and Z_k^l which can react according to the following bimolecular reaction:

$$\mathcal{Z}_i + \mathcal{Z}_k \xrightarrow{\kappa} \mathcal{Z}_m.$$

Then a suitable probability of reaction per time step gives the corresponding macroscopic rate of reaction [6]. This probability is a function of the distance $|\mathbf{x}_{i,j} - \mathbf{x}_{k,l}|$ between reacting molecules. Models postulate that the molecules can only react if they are within a specific distance (reaction radius) [3]. Care must also be taken when generating the initial positions of products of chemical reactions. This is especially the case whenever reversible reactions are present in the system. If the molecules are not initialized properly, then the products may unphysically react immediately after being created [24, 22]. The GFRD algorithm, for example, requires molecules that are involved in reversible reactions to be placed a distance x_{sep} from each other [32]. Each time a reaction occurs x_{sep} is sampled from a specific probability distribution.

1.2.2. Boundary conditions. Molecules that migrate over domain boundaries are treated depending on whether they are reflective, absorbing, or reactive boundaries [5]. When modeling boundary conditions, one has to take into account that (1.7) is only an approximation of the Brownian motion (1.8). Let us consider that the formula (1.7) gives the updated position of the molecule Z_i^j inside the domain Ω_M, i.e., $\mathbf{x}_{i,j}(t + \Delta t) \in \Omega_M$. Then there is still a nonzero probability that the molecule (which follows (1.8)) left the domain Ω_M during the time $(t, t+\Delta t)$ and then returned to Ω_M. We denote this probability by $P_m \equiv P_m(\mathbf{x}_{i,j}(t), \mathbf{x}_{i,j}(t + \Delta t))$. Near a flat boundary $\partial\Omega_M$, probability P_m takes the analytical form

$$P_m = \exp\left(\frac{-\text{dist}(\mathbf{x}_{i,j}(t), \partial\Omega_M)\ \text{dist}(\mathbf{x}_{i,j}(t + \Delta t), \partial\Omega_M)}{D_i \Delta t}\right), \tag{1.9}$$

where $\text{dist}(\cdot, \partial\Omega_M)$ represents the distance from the boundary $\partial\Omega_M$ [3]. While boundaries are sometimes only implemented at time $t + \Delta t$ for molecule Z_i^j if $\mathbf{x}_{i,j}(t + \Delta t)$ computed by (1.7) is outside Ω_M, thorough implementation of boundary conditions should be considered not only when $\mathbf{x}_{i,j}(t + \Delta t) \notin \Omega_M$ but also with the probability P_m if $\mathbf{x}_{i,j}(t + \Delta t) \in \Omega_M$. No closed form solution exists for P_m for irregular boundary geometries $\partial\Omega_M$. In practice, a curved boundary is usually described locally by a flat approximation which increasingly becomes more accurate for small values of Δt [3].

1.3. The two regime method. The TRM for simulation of stochastic reaction-diffusion processes is characterized by its partition of the computational domain $\Omega \subset \mathbb{R}^N$, $N = 1, 2, 3$, into two nonoverlapping open subsets Ω_C and Ω_M, i.e., $\Omega_C \cap \Omega_M = \emptyset$ and $\overline{\Omega}_C \cup \overline{\Omega}_M = \overline{\Omega}$, where overbars denote the closure of the corresponding set. We denote by I the interface between the subdomains Ω_C and Ω_M, i.e., $I = \partial\Omega_C \cap \partial\Omega_M$. Internally, molecules are simulated in subdomains Ω_C and Ω_M by compartment-based and molecular-based approaches which were described in sections 1.1 and 1.2, respectively. Molecules in Ω_M are updated at prescribed times separated by Δt. Meanwhile, molecules in Ω_C are updated at the events determined by compartment-based modeling rules described in section 1.1. The simulation is

thus built from a series of time steps that occur at each "regular time step" separated by Δt and each event inside Ω_C. As the time updates can be classified by the region that they apply to, updates corresponding to compartment-based events are known as C-events (or compartment events) and the regular updates separated by Δt in time are known as M-events. There are several possible variants of the TRM [10]. In this paper, we will analyze the TRM in the form which is summarized in Figure 1. In step **(i)**, we define Ω_C, Ω_M and the time step Δt. Initial conditions in Ω_M and Ω_C are implemented in steps **(ii)** and **(iii)**, respectively. In step **(iv)**, we also define putative times t_M and t_C when the next M-event and C-event will occur, respectively. Then the TRM repeats steps **(v)** and **(vi)** until the desired end of the simulation. Molecules which cross the interface are only placed on the other side of the interface at the next M-event and not at intermediate C-events. The master equation which is used in section 2 to analyze the coupling rules and their impact on the local molecule distribution is valid if molecules move over the interface at intervals of Δt.

1.3.1. Transition of molecules from Ω_C to Ω_M. The partition of the domain into Ω_C and Ω_M is an artificial partitioning that should not interfere with the natural diffusion of molecules in the domain. To describe migration of molecules from Ω_C to Ω_M, we need an expression for the propensity of molecules to jump from compartments $\mathcal{C}_j$, adjacent to the interface I, into Ω_M. When a molecule successfully jumps from $\mathcal{C}_j$ into Ω_M, it must be placed with a specific set of coordinates by virtue of the modeling approach in Ω_M. For a regular array of square or cubic compartments in Ω_C, we define the propensity of chemical species $\mathcal{Z}_i$ to jump from $\mathcal{C}_j$ into Ω_M to be some multiple $\Phi_{i,j}$ times the natural jumping propensity between neighboring compartments (provided that compartment $\mathcal{C}_j$ is adjacent to I, a so-called interfacial compartment; otherwise this propensity is equal to 0). That is (compare with (1.6)),

$$\alpha_{\mathcal{D},i,j,M} = \Phi_{i,j} \frac{D_i}{h^2} \mathcal{N}_{i,j}, \tag{1.10}$$

where the index j is a reference to the originating interfacial compartment $\mathcal{C}_j$. Subsequently, the molecule, after being chosen to jump from $\mathcal{C}_j$ into Ω_M is initialized at a position $\mathbf{x} \in \Omega_M$. We do not restrict this initialization to a specific location but rather consider that the initial position is chosen from a probability distribution $f_{i,j}(\mathbf{x})$.

1.3.2. Transition of molecules from Ω_M to Ω_C. In step (vi) in Figure 1, a molecule originating in Ω_M is transferred into Ω_C with a probability $\Psi \in [0,1]$ if the molecule interacted with the interface I within the time interval $[t, t+\Delta t]$. It is postulated that molecule Z_i^j interacted with I if one of these two conditions is satisfied:

(a) $\mathbf{x}_{i,j}(t+\Delta t)$ computed by (1.7) satisfies $\mathbf{x}_{i,j}(t+\Delta t) \in \Omega_C$.

(b) $\mathbf{x}_{i,j}(t+\Delta t) \in \Omega_M$ and $r \le P_m$, where r is a uniformly distributed random number in $(0,1)$ and $P_m \equiv P_m(\mathbf{x}_{i,j}(t), \mathbf{x}_{i,j}(t+\Delta t))$ was introduced in section 1.2.2. For a straight interface I, the probability P_m is given by (1.9).

If the probability Ψ is strictly less than 1, then we have to incorporate into the TRM that all molecules which satisfy (a) and which are not transported to Ω_C are reflected back to Ω_M. However, this condition is not necessary in one dimension, where it is possible to prove that $\Psi = 1$ [10]. This simplifies the implementation of the TRM in one dimension. In the next section, we summarize the results of the 1D theory presented in [10]. Then, in section 2, we analyze the TRM in two dimensions.

(i) Define the subdomains Ω_C and Ω_M and the interface $I = \partial\Omega_C \cap \partial\Omega_M$. Subdivide Ω_C into compartments $\mathcal{C}_j$, $j = 1, \ldots, K$. Choose the time step Δt between updates of the molecular-based regime (M-events) in Ω_M.

(ii) Specify the initial condition in Ω_M by placing molecules Z_i^j in Ω_M at initial positions $\mathbf{x}_{i,j}(0) \in \Omega_M$, $i = 1, 2, \ldots, M$, $j = 1, 2, \ldots, n(i)$, where $n(i)$ is the initial number of molecules of the ith chemical species $\mathcal{Z}_i$ in Ω_M.

(iii) Specify the initial condition in Ω_C by initializing the copy numbers $\mathcal{N}_{i,j}$ in Ω_C for each chemical species $\mathcal{Z}_i$ in each compartment $\mathcal{C}_j$, $i = 1, 2, \ldots, M$, $j = 1, 2, \ldots, K$. Initialize time as $t := 0$.

(iv) Use (1.1) to calculate $t_{\mathcal{E}}$, the putative times at which all C-events $\mathcal{E}$ will take place. Set $t_M = \Delta t$ and $t_C = \min_{\mathcal{E}} t_{\mathcal{E}}$, where the minimum is taken over all possible C-events $\mathcal{E}$.

(v) If $t_C \leq t_M$, then the next C-event occurs:

- Update current time $t := t_C$.
- Change the number of molecules in Ω_C to reflect the specific C-event that has occured. If this event is one in which a molecule of chemical species $\mathcal{Z}_i$ leaves Ω_C bound for Ω_M, then compute its initial position in Ω_M according to the probability distribution $f_{i,j}(\mathbf{x})$ and remove it from the corresponding compartment $\mathcal{C}_j$.
- Calculate the next putative time for the current C-event by (1.1). For all propensity functions $\alpha_{\mathcal{E}}$ that are changed as a result of the C-event, determine the putative times of the corresponding event by (1.2).
- Set $t_C := \min_{\mathcal{E}}(\tau_{\mathcal{E}})$.

(vi) If $t_M \leq t_C$, then the next M-event occurs:

- Update current time $t := t_M$.
- Change the locations of all molecules in Ω_M using (1.7).
- Implement boundary conditions at the external boundary $\partial\Omega_M \backslash I$.
- Initialize all molecules which migrated from Ω_C to Ω_M since the previous M-event at locations computed in the step (v) according to $f_{i,j}(\mathbf{x})$.
- Perform all reaction events in Ω_M.
- Identify all molecules that interact with the interface I from Ω_M (excluding those just initiated) using conditions (a)–(b) from section 1.3.2. Move each molecule into the appropriate compartment in Ω_C with probability Ψ. Otherwise, its position is reflected back to Ω_M.
- For all propensity functions $\alpha_{\mathcal{E}}$ that are changed as a result of the M-event determine the putative times of the corresponding C-event by (1.2).
- Update $t_M := t_M + \Delta t$ and, if necessary, set $t_C := \min_{\mathcal{E}}(\tau_{\mathcal{E}})$.

(vii) Repeat steps (v) and (vi) until the desired end of the simulation.

FIG. 1. *The pseudocode of the TRM for stochastic reaction-diffusion simulation.*

1.3.3. Summary of analysis of the TRM in one dimension. In [10], the TRM is presented and analyzed in a 1D domain $\Omega = (-\infty, \infty)$ which was divided by the interface $I = \{0\}$ into $\Omega_C = (-\infty, 0)$ and $\Omega_M = (0, \infty)$. The subdomain Ω_C was divided into compartments of the same length h, i.e., $\mathcal{C}_j = (-jh, (1-j)h)$, $j = 1, 2, \ldots$. In this case, there is only one interfacial compartment corresponding to $j = 1$ and coordinates $x \in \Omega_M$ are defined as the displacement from the interface I. It was obtained that

$$\Phi_{i,1} = \frac{2h}{\sqrt{\pi D_i \Delta t}}, \qquad \Psi = 1, \tag{1.11}$$

$$f_{i,1}(x) = \sqrt{\frac{\pi}{4D_i\Delta t}}\,\mathrm{erfc}\left(\frac{x}{\sqrt{4D_i\Delta t}}\right), \qquad x \in \Omega_M, \tag{1.12}$$

where $\mathrm{erfc}(x) = 2/\sqrt{\pi}\int_x^\infty \exp(-t^2)\mathrm{d}t$ is the complementary error function. These formulas were derived under the assumption $D_i\Delta t \sim h^2$ as $h \to 0$, a condition which is used throughout the manuscript. If Δt gets larger than this, then the expected jump distance of molecules in the Brownian domain, $\sqrt{2D_i\Delta t}$, becomes greater than the compartment size h. Since in the simplest form of the TRM scheme we do not allow Brownian particles to jump to interior compartments (particles that cross the interface are placed in a boundary compartment), we often assume $D_i\Delta t < h^2$. (We are usually interested in a finer resolution in the Brownian domain than the compartment domain.) If multiple species are involved in the same simulation, each with a different diffusion constant, Δt should be chosen so that all species satisfy this inequality.

If $D_i\Delta t$ is chosen much smaller than h^2, then the coupling between domains is still accurate in one dimension. However, we will see that when $\sqrt{2D_i\Delta t} \ll h$ in higher dimensions care needs to be taken to avoid numerical artifacts associated with molecules diffusing along the interface I.

2. Two-regime coupling in dimensions greater than one. In the rest of this paper we wish to derive forms for $\Phi_{i,j}$, Ψ, and $f_{i,j}(\mathbf{x})$ in domains with dimensions greater than $N = 1$.

Until now, we have used the index i to denote the chemical species of the molecule which is being simulated. This is because tracking the chemical species is very important for correctly identifying reactions and diffusive motion. Correct coupling over and interface using the TRM involves the careful placement of molecules as they migrate over the interface in such a way that, locally, it appears as though the interface is not there. This means that our analysis only needs to consider the spatial coupling of a single molecule and we do not need to note the chemical species in our analysis (since methodologies for reaction in each respective regime are well established and depend on specific algorithms chosen by the modeler). We shall therefore drop the index i and relabel D_i as D, which will denote the diffusion constant for the chemical species in question. Our aim is therefore to find the parameters Φ_j, Ψ, and $f_j(\mathbf{x})$ for domains that have more than one dimension.

We shall limit the analysis to regularly spaced square compartments of length h for dimension $N = 2$, but the results can be easily generalized to regularly spaced N-dimensional cubic compartments (see section 2.3). The parameters will be derived for a flat interface I and then we will discuss the case where I may have a corner.

2.1. Matching at a flat interface in two dimensions. The considered geometry is represented graphically in Figure 2. We present here a derivation of the parameters Φ_j, Ψ, and $f_j(\mathbf{x})$ for the TRM applied to an infinite two-dimensional domain $\Omega = \mathbb{R}^2$ and a single flat interface I. To derive these algorithm parameters (and formulate them in a reasonably simplified form), we denote by (x, y) the Cartesian coordinates that describe domain Ω. Without loss of generality we assign Ω_M to the region defined by $x > 0$ and therefore Ω_C to the region defined by $x < 0$ (i.e., the interface I is the line $x = 0$). The compartments $\mathcal{C}_j$ are regularly spaced squares of side length h. We find it convenient to describe the compartments by two indices such that each compartment $\mathcal{C}_{i,j}$ is assigned to the region described by $-(i+1)h < x < -ih$ and $jh - h/2 < y < jh + h/2$, where $i \in \mathbb{N}_0$ and $j \in \mathbb{Z}$. In what follows, we will denote

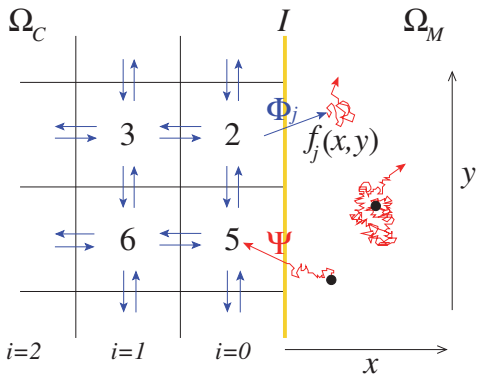

FIG. 2. *Graphical representation of the TRM in two dimensions for a flat interface I. The compartment-based regime Ω_C is on the left (numbers denote an example of the number of molecules in the corresponding compartment), and the molecular-based regime Ω_M on the right (three illustrative trajectories of individual molecules are plotted as red lines). The interface I is plotted as a yellow line.*

by $p_{i,j}(t)h^2$ the probability a molecule will be in the compartment $\mathcal{C}_{i,j}$, i.e., $p_{i,j}(t)$ is the (discretized, averaged) probability density in the compartment $\mathcal{C}_{i,j}$.

Since the analysis of the TRM only depends on the properties of diffusion [10], we can write the governing equations as the evolution equations for the probability density of a single diffusing molecule in Ω. The goal of the TRM is to correctly approximate its probability density function $P(x, y, t)$, where $(x, y) \in \Omega$ and time $t \geq 0$. Using (1.6), (1.7), (1.9), (1.10), and the description of the evolution of molecules near the interface I during the TRM, the TRM master equations for both the average probability density $p_{0,n}(t)$ for a molecule to be in the $\mathcal{C}_{0,n}$ compartment and the probability density $p(x, y, t)$ in Ω_M can be constructed in a similar way to that described in [10]. They are given by

(2.1)
$$p_{0,n}(t+\Delta t) = \left(1 - \frac{(3+\Phi_0)D\Delta t}{h^2}\right) p_{0,n}(t) + \frac{D\Delta t}{h^2}\left(p_{0,n-1}(t) + p_{0,n+1}(t) + p_{1,n}(t)\right) + \frac{2\Psi}{h^2}\int_{nh-h/2}^{nh+h/2} \mathrm{d}y \int_{-\infty}^{\infty} \mathrm{d}\bar{y} \int_{0}^{\infty} \mathrm{d}x \int_{0}^{\infty} \mathrm{d}\bar{x}\; p(\bar{x}, \bar{y}, t) K\left(x + \bar{x}\right) K\left(y - \bar{y}\right),$$

(2.2)
$$p(x, y, t+\Delta t) = \int_{-\infty}^{\infty} \mathrm{d}\bar{y} \int_{0}^{\infty} \mathrm{d}\bar{x}\; p(\bar{x}, \bar{y}, t) \left[K\left(x - \bar{x}\right) + (1 - 2\Psi) K\left(x + \bar{x}\right)\right] K\left(y - \bar{y}\right) + D\Delta t \sum_{j \in \mathbb{Z}} \Phi_j f_j(x, y) p_{0,j}(t),$$

where $K(x) = (4\pi D\Delta t)^{-1/2} \exp(-x^2/(4D\Delta t))$ is the distribution of the random displacement in the position of molecules between t and $t + \Delta t$ given by (1.7). One key assumption that is made in (2.1) is that molecules that are absorbed into Ω_C from Ω_M are absorbed into the closest compartment $\mathcal{C}_{0,j}$ to their position calculated at $t + \Delta t$. (See the limits of integration over the variable y in (2.1).) It can also be shown [5, 10] that the contributions of the two ways a molecule may be absorbed by the interfacial compartment (see cases (a)–(b) in section 1.3) to the total number of

absorbed molecules in a time step are equal giving rise to the factor of 2 in the integral term on the right-hand side of (2.1) and the absorption component of the integral on the right-hand side of (2.2).

We may further simplify (2.1)–(2.2) by using the symmetry of the domain in the y-direction. First, since Φ_j (where j refers to compartments $\mathcal{C}_{0,j}$ on the interface) is dependent only on the morphology of $\mathcal{C}_{0,j}$ and its relative position to I, we expect Φ_j to be independent of j and we therefore denote

$$\Phi_j \equiv \Phi. \tag{2.3}$$

Second, symmetry in the y-direction also allows us to make the conclusion that

$$f_j(x,y) = f_0(x, y - jh), \tag{2.4}$$

where the index of f_j refers only to interfacial compartments $\mathcal{C}_{0,j}$.

In the vicinity of $x = 0$ there is a boundary layer of width $O(\sqrt{\Delta t})$ [5, 10]. We rescale (2.1)–(2.2) using the dimensionless boundary layer coordinate $x = \xi\sqrt{D\Delta t}$. We also denote the probability density and placement function in this boundary layer region by $p_{\text{in}}(\xi, y, t)$ and $f_{\text{in},j}(\xi, y) = \sqrt{D\Delta t}\, f_j(\xi\sqrt{D\Delta t}, y)$. The rescaling of f_j is necessary to satisfy the normalization condition

$$\int_{-\infty}^{\infty}\int_{0}^{\infty} f_j(x,y)\ \mathrm{d}x\ \mathrm{d}y = 1$$

since (as we will see) f_j vanishes outside of the boundary layer. Thus, using (2.3) and (2.4), in the boundary layer coordinates (2.1)–(2.2) become

$$\begin{aligned} p_{0,n}(t+\Delta t) = {} & \left(1 - \frac{(3+\Phi)}{\Lambda^2}\right) p_{0,n}(t) + \frac{1}{\Lambda^2}\big(p_{0,n-1}(t) + p_{0,n+1}(t) + p_{1,n}(t)\big) \\ & + \frac{2\Psi}{h\Lambda}\int_{nh-h/2}^{nh+h/2}\mathrm{d}y\int_{-\infty}^{\infty}\mathrm{d}\bar{y}\int_{0}^{\infty}\mathrm{d}\xi\int_{0}^{\infty}\mathrm{d}\bar{\xi}\, p_{\text{in}}(\bar{\xi},\bar{y},t)\,\kappa\left(\xi+\bar{\xi}\right) K\left(y-\bar{y}\right), \end{aligned} \tag{2.5}$$

$$\begin{aligned} p_{\text{in}}(\xi, y, t+\Delta t) = {} & \int_{-\infty}^{\infty}\mathrm{d}\bar{y}\int_{0}^{\infty}\mathrm{d}\bar{\xi}\ p_{\text{in}}(\bar{\xi},\bar{y},t)\left[\kappa\left(\xi-\bar{\xi}\right) + (1-2\Psi)\kappa\left(\xi+\bar{\xi}\right)\right] K\left(y-\bar{y}\right) \\ & + \sqrt{D\Delta t}\,\Phi\sum_{j\in\mathbb{Z}} f_{\text{in},0}(\xi, y-jh)\, p_{0,j}(t), \end{aligned} \tag{2.6}$$

where $\Lambda = h/\sqrt{D\Delta t}$ and $\kappa(\xi) = \sqrt{D\Delta t}\, K(\sqrt{D\Delta t}\,\xi) = (4\pi)^{-1/2}\exp(-\xi^2/4)$. Let us denote $\bar{p}(y,t) = P(0,y,t)$ and $\bar{p}_x(y,t) = P_x(0,y,t)$, where $P(x,y,t)$ is the distribution which the TRM approximates (for $x \in \mathbb{R}$ and $y \in \mathbb{R}$). In order for the models to join smoothly at the interface I we require on the compartment-based side that

$$\begin{aligned} p_{0,n}(t) &\sim P(0, nh, t) = \bar{p}(nh, t), \\ p_{1,n}(t) &\sim P(-h, nh, t) = \bar{p}(nh, t) - h\bar{p}_x(nh, t) + O(h^2), \\ p_{0,n+1}(t) &\sim P(0, nh+h, t) = \bar{p}(nh+h, t), \\ p_{0,n-1}(t) &\sim P(0, nh-h, t) = \bar{p}(nh-h, t), \end{aligned} \tag{2.7}$$

while, for the molecular-based side, we require no rapid variation in the boundary layer, so that

$$p_{\text{in}}(\xi, y, t) \sim \bar{p}(y,t) + \sqrt{D\Delta t}(\xi + C_x)\bar{p}_x(y,t) + \cdots, \tag{2.8}$$
$$p_{\text{in}}(\xi, y, t+\Delta t) \sim \bar{p}(y,t+\Delta t) + \sqrt{D\Delta t}(\xi + C_x)\bar{p}_x(y,t) + \cdots,$$

where we have allowed for a small shift C_x in which the molecular-based region "sees" the interface [10]. Similarly

$$\int_{-\infty}^{\infty} K(y-\bar{y})\,\bar{p}(\bar{y},t)\,\mathrm{d}\bar{y} = \bar{p}(y,t) + O(\Delta t).$$

Substituting the expansions (2.7)–(2.8) into (2.5) and (2.6), using $h \sim \sqrt{D\Delta t}$ as $h \to 0$ and $\Delta t \to 0$, we obtain

$$\begin{aligned} 0 = &-\frac{\Phi}{\Lambda^2}\bar{p}(nh,t) + \frac{1}{\Lambda^2}h\bar{p}_x(nh,t) \\ &+ \frac{2\Psi}{\Lambda}\frac{1}{\sqrt{\pi}}\bar{p}(nh,t) + \frac{2\Psi}{\Lambda}\sqrt{D\Delta t}\left(\frac{1}{2} + \frac{C_x}{\sqrt{\pi}}\right)\bar{p}_x(nh,t) + O(h^2), \end{aligned} \tag{2.9}$$

$$\begin{aligned} 0 = &-\Psi\,\mathrm{erfc}\left(\frac{\xi}{2}\right)\bar{p}(y,t) \\ &+ \sqrt{D\Delta t}\left(\frac{(2-2\Psi)}{\sqrt{\pi}}e^{-\xi^2/4} - C_x\Psi\mathrm{erfc}\left(\frac{\xi}{2}\right) + (\Psi-1)\xi\mathrm{erfc}\left(\frac{\xi}{2}\right)\right)\bar{p}_x(y,t) \\ &+ \sqrt{D\Delta t}\,\Phi\sum_{j\in\mathbb{Z}} f_{\text{in},0}(\xi, y-jh)\,\bar{p}(jh,t) + O(h^2). \end{aligned} \tag{2.10}$$

Equating coefficients of $\bar{p}(nh,t)$ and $\bar{p}_x(nh,t)$ in (2.9) gives

$$\Phi = \frac{2\Psi\Lambda}{\sqrt{\pi}}, \qquad 1 = \Psi\left(1 + \frac{2C_x}{\sqrt{\pi}}\right). \tag{2.11}$$

From the coefficient of $\bar{p}_x$ in (2.10) we see that

$$\Psi = 1 \quad \text{and} \quad C_x = 0. \tag{2.12}$$

Consequently, (2.11) implies that Φ satisfies (1.11). Using (2.12) and (2.10) we find that $f_{\text{in},0}$ has to satisfy

$$\mathrm{erfc}\left(\frac{\xi}{2}\right)\bar{p}(y,t) = \frac{2h}{\sqrt{\pi}}\sum_{j\in\mathbb{Z}} f_{\text{in},0}(\xi, y-jh)\,\bar{p}(jh,t) + O(h^2).$$

Writing

$$f_{\text{in},0}(\xi, y) = \frac{\sqrt{\pi}}{2}\mathrm{erfc}\left(\frac{\xi}{2}\right)F(y),$$

this becomes

$$\bar{p}(y,t) = h\sum_{j\in\mathbb{Z}} F(y-jh)\,\bar{p}(jh,t) + O(h^2). \tag{2.13}$$

This is a standard interpolation problem. The simplest weight function which gives $O(h^2)$ accuracy is the triangle function

$$F(y) = \begin{cases} \frac{1}{h}\left(1 - \frac{|y|}{h}\right) & \text{for } -h < y < h, \\ 0 & \text{otherwise.} \end{cases} \tag{2.14}$$

Thus

$$f_0(x,y) = \begin{cases} \frac{1}{h}\sqrt{\frac{\pi}{4D\Delta t}}\,\operatorname{erfc}\left(\frac{x}{\sqrt{4D\Delta t}}\right)\left(1 - \frac{|y|}{h}\right) & \text{for } -h < y < h, \\ 0 & \text{otherwise.} \end{cases} \tag{2.15}$$

It is important to note that our expansions (2.7) assume that the probability $p_{i,j}$ of being in compartment $\mathcal{C}_{i,j}$ should be a continuous extension of $p(x,y)$ evaluated at $(-ih, jh)$ which is in the center of the right side of the compartments. If the expansions (2.7) were taken in the center of the compartments (evaluated at $(-ih - h/2, jh)$) the result would be that $C_1 = -\Lambda/2$ and thus a shift in the continuous expected probability density curve over the interface is seen resulting in an apparent error of $h\bar{p}_x/2 + O(h^2)$ as $\Delta t \to 0$ on the interface [10]. This error can therefore be reduced by refining the lattice (compartments) near the interface (remembering that this might mean also reducing Δt such that $D\Delta t \sim h^2$).

The derivation above was conducted under the assumption $D\Delta t \sim h^2$. Let us now assume $D\Delta t \ll h^2$ instead. Then $\Lambda = h/\sqrt{D\Delta t}$ and Φ (given by (1.11) as $2\Lambda/\sqrt{\pi}$) are no longer of order 1, and the above derivation may fail. In particular, we retain terms of order h while ignoring terms of order Φh^2. If we are interested in very small Δt the errors associated with this mismatch between Δt and h may be reduced by replacing $F(y)$ by the step function

$$\bar{F}(y) = \begin{cases} \frac{1}{h} & \text{for } -h/2 < y < h/2, \\ 0 & \text{otherwise,} \end{cases} \tag{2.16}$$

which gives $O(h)$ accuracy to (2.13). This function is also easier to implement in the case of corners which will be discussed in the next section. Using (2.16) instead of (2.14), (2.15) reads as follows:

$$f_0(x,y) = \begin{cases} \frac{1}{h}\sqrt{\frac{\pi}{4D\Delta t}}\,\operatorname{erfc}\left(\frac{x}{\sqrt{4D\Delta t}}\right) & \text{for } -h/2 < y < h/2, \\ 0 & \text{otherwise.} \end{cases} \tag{2.17}$$

These issues will be discussed further in section 3.

2.2. Interface corners. The analysis in the previous section does not extend trivially to the case when there are corners in the interface I. Indeed, when the interface is not perfectly flat the previous section is invalid. However, since we are restricting our analysis to regular cubic lattices in Ω_C, the interface must be made up of a series of straight edges connected at right angles. Let us consider the compartments $\mathcal{C}_{i,j}$ assigned to the region $((i-1)h, ih) \times ((j-1)h, jh)$, where the indices

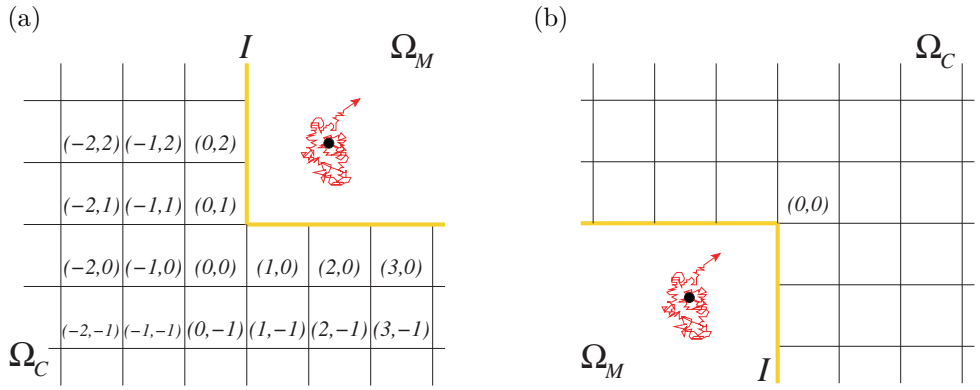

FIG. 3. (a) *Illustration of corner geometry in two dimensions. Compartment indices are denoted as in section* 2.2. (b) *The corner geometry used in illustrative numerical simulations in section* 3.2.

$(i, j) \in \mathbb{Z} \times \mathbb{Z} \backslash \mathbb{N} \times \mathbb{N}$ (i.e., they fill the complement of the positive quadrant). The considered geometry is represented graphically in Figure 3(a).

Molecules cannot leave compartment $\mathcal{C}_{0,1}$ using (2.14). This is because there is a nonzero probability that the molecule crosses diagonally to the region of $\mathcal{C}_{1,0}$ and vice versa. This diagonal movement is prohibited by the rules of the compartment-based region but is allowed in the molecular region. Furthermore, molecules in Ω_M may move into $\mathcal{C}_{0,0}$ during one time step. Typically, molecules in compartments will not be able to move diagonally out of $\mathcal{C}_{0,0}$. While it may be possible to make diagonal motion an exception for $\mathcal{C}_{0,0}$, atypical functions placing molecules into Ω_M from $\mathcal{C}_{0,0}$, $\mathcal{C}_{0,1}$, and $\mathcal{C}_{1,0}$ must be determined and also rules for how molecules in Ω_M close to the corner migrate diagonally, left, or down into Ω_C must be determined. It is important to note that the added complexity to these corner compartments is not as simple as the case when the compartments form a straight interface. If we attempted to generalize (2.14), then complex distributions would have to be sampled from to place molecules from $\mathcal{C}_{0,1}$ and $\mathcal{C}_{1,0}$ into Ω_M and several tests would have to be performed on molecules in Ω_M (to see if they meet criteria for diagonal migration into Ω_C, or to determine if they move down or left over the interface). Given this complication, we find it reasonable to use (2.16) instead of (2.14), which means that we use (2.17) instead of (2.15). Distribution (2.17) does not allow for molecules to leak between $\mathcal{C}_{0,1}$ and $\mathcal{C}_{1,0}$ but at the cost of accuracy in the local region around the corner.

The treatment of molecules at the corner is therefore described by the following rules. Molecules in compartments $\mathcal{C}_{0,1}$ and $\mathcal{C}_{1,0}$ have the propensities given by (1.10), namely,

$$\Phi \frac{D}{h^2} \mathcal{N}_{0,1}, \qquad \Phi \frac{D}{h^2} \mathcal{N}_{1,0},$$

where $\mathcal{N}_{0,1}$ (resp., $\mathcal{N}_{1,0}$) is the number of molecules in the compartment $\mathcal{C}_{0,1}$ (resp., $\mathcal{C}_{1,0}$). Molecules from $\mathcal{C}_{0,0}$ may not enter Ω_M directly. Molecules from Ω_M that land in $\mathcal{C}_{0,0}$ or satisfy condition (b) in section 1.3.2 for both parts $\{x = 0\}$ and $\{y = 0\}$ of the interface I are placed at random (with probability 1/2) in $\mathcal{C}_{1,0}$ or $\mathcal{C}_{0,1}$. Molecules in the compartment $\mathcal{C}_{0,1}$ migrating to Ω_M are placed according to the distribution (2.17). Molecules in the compartment $\mathcal{C}_{1,0}$ migrating to Ω_M are placed according to the distribution

$$f_0(x,y) = \begin{cases} \dfrac{1}{h}\sqrt{\dfrac{\pi}{4D\Delta t}}\,\mathrm{erfc}\left(\dfrac{y}{\sqrt{4D\Delta t}}\right) & \text{for } -h/2 < x < h/2, \\ 0 & \text{otherwise,} \end{cases} \tag{2.18}$$

which can be obtained from the distribution (2.17) by exchanging the variables x and y. Thus, in both cases, we use (1.12) perpendicular from their respective interfaces and the step distribution (2.16) tangentially along each respective interface.

Since $D\Delta t < h^2$ molecules that are in compartments $\mathcal{C}_{i,0}$ and $\mathcal{C}_{0,j}$ $(i,j \geq 2)$ are not significantly affected by the corner within one time step. We therefore use the probability distribution (2.17) for these compartments. Thus we use the distribution (2.16) for molecules leaving the corner compartments and the triangle distribution (2.14) for molecules leaving all other boundary compartments.

Finally, we note that we also tested the alternative of using a one-sided triangle distribution for the corner compartments $\mathcal{C}_{1,0}$ or $\mathcal{C}_{0,1}$. It produced results which were indistinguishable statistically from those generated using (2.16) for the example shown in section 3.2.

Incidentally, these same heuristic arguments extend to the situation when Ω_C fills one quadrant and Ω_M fills three quadrants. Perpendicular positioning of a molecule exiting the compartment-based regime at the corner is carried out according to (1.12) perpendicular to each interface and the step distribution (2.16) tangentially along each interface.

2.3. Parameters for a flat interface in N dimensions. The derivation presented in section 2.1 can be used for flat interfaces in arbitrary dimensions. One can show that the parameters $\Phi_j = \Phi$ and Ψ are independent of the number of dimensions N of the domain for a flat interface with a regular cubic lattice arrangement in Ω_C (and therefore take the values derived in section 2.1). Furthermore one can show that the distribution $f_0(\mathbf{x})$ for placing molecules in Ω_M is the product of N distributions separating the coordinates

$$f_0(x_1, x_2, \ldots, x_N) = F^{\perp}(x_1) \prod_{i=2}^{N} F^{\parallel}(x_i). \tag{2.19}$$

Here, the distribution $F^{\perp}(x_1)$ is for the coordinate x_1 perpendicular to the interface $I = \{x_1 = 0\}$. It is given (see (1.12) and (2.15)) by

$$F^{\perp}(x_1) = \sqrt{\frac{\pi}{4D\Delta t}}\mathrm{erfc}\left(\frac{x_1}{\sqrt{4D\Delta t}}\right). \tag{2.20}$$

The remaining $N-1$ identical distributions for each coordinate x_i, $i = 2, \ldots, N$, tangential to the interface I, are denoted as $F^{\parallel}(x_i)$ in (2.19). If the origin is placed at the center of compartment in question, then one can follow the derivation presented in section 2.1 to obtain $F^{\parallel}(x_i) = F(x_i)$ given by (2.14). Equation (2.19) indicates that tangential coordinates should be chosen independently from each other. Indeed, by extention of this property, being able to treat right-angle corners and straight edges in two dimensions allows us to describe many different types of corner geometries in higher dimensions.

3. Illustrative numerical examples. The location and geometry of the interface that is constructed between mesoscopic and microscopic simulation regimes

is entirely dependent on the application and is to be chosen for optimal numerical convenience. For example, when the microscopic region of interest is in the vicinity of a reacting target on a polymer or membrane, the interface that should be used is one that encapsulates this region. While a sphere or dome could be used, this would necessitate irregularly shaped mesoscopic lattices. We recommend, where possible, that the interface be made up of straight lines meeting at right angles. This is done in such a way that a regular lattice may be used.

In this section we present simple diffusion simulations using the TRM to demonstrate its accuracy and convergence. We present test problems that particularly pertain to straight interfaces with right-angle corners. We emphasize, in particular, a comparison between using distributions (2.15) and (2.17) for molecules migrating across the interfaces.

We have chosen not to include reactions or complicated biological behavior in these test problems in order to keep the presentation as clear as possible. Although reaction rates are sensitive to diffusion, if diffusion across the interface is modeled correctly, correct reaction rates will follow. This has been noted particularly for the TRM in a number of examples [11, 8].

3.1. Straight interface. We will consider a diffusing molecule which starts at the origin at (dimensionless) time $t = 0$ and diffuse with (dimensionless) diffusion constant $D = 1$ in the semi-infinite two-dimensional domain $\Omega = (0, \infty) \times (0, \infty)$. Boundary $\partial\Omega$ will be considered reflective.

The probability distribution, $P(x, y, t)$, to find the molecule at time t given its initial position at the origin evolves according to the PDE

$$\frac{\partial P}{\partial t} = \frac{\partial^2 P}{\partial x^2} + \frac{\partial^2 P}{\partial y^2} \tag{3.1}$$

with the initial condition $P(x, y, 0) = \delta(x, y)$, where δ is the Dirac delta function. Using no-flux (reflective) boundary condition ($\nabla P \cdot \hat{\mathbf{n}} = 0$), (3.1) can be solved as

$$P(x, y, t) = \frac{1}{\pi t} \exp\left(\frac{-(x^2 + y^2)}{4t}\right). \tag{3.2}$$

We shall simulate this diffusion process stochastically using the TRM where Ω is divided into

$$\Omega_M = (0, 0.5) \times (0, \infty) \qquad \text{and} \qquad \Omega_C = (0.5, \infty) \times (0, \infty). \tag{3.3}$$

We run $N_0 = 2 \times 10^5$ realizations of the TRM for the molecule starting at the origin and note its state (in either the molecular-based regime or the compartment-based regime) at each time step until $t = 1$. We simulate the compartment regime using at each time step until $t = 1$. We simulate the compartment-based regime using a square lattice with nondimensional compartment spacings $h = 0.05$, $h = 0.1$, and $h = 0.25$. We choose $h = 0.25$, a very coarse discretization, to emphasize the error that is introduced by a coarse lattice discretization. Since our analysis uses the assumption $D\Delta t \sim h^2$, we use the time steps $\Delta t = 0.0004$, $\Delta t = 0.0016$, and $\Delta t = 0.01$, respectively, with $D = 1$ such that $h/\sqrt{D\Delta t} = 2.5 \sim O(1)$.

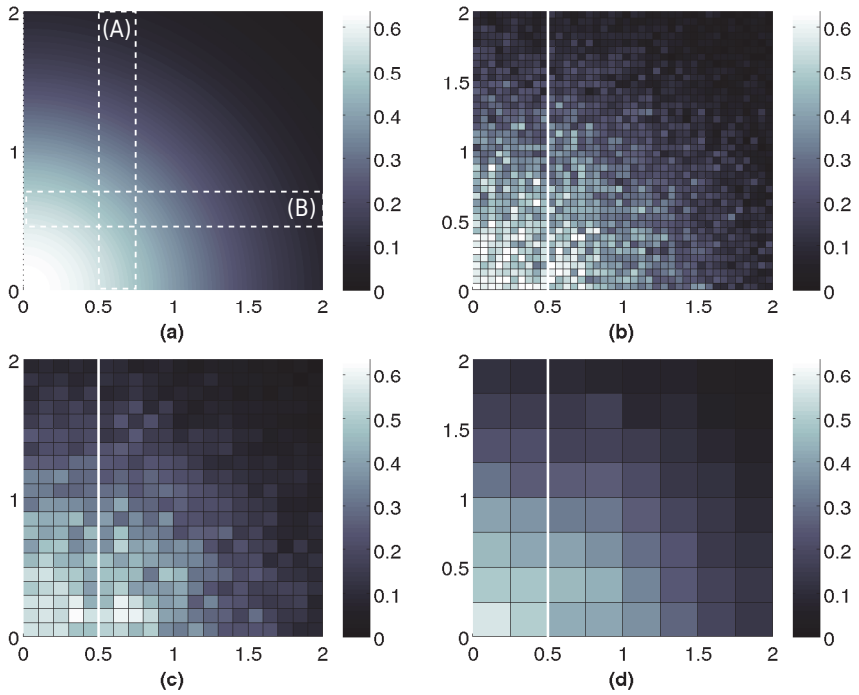

FIG. 4. *Probability distribution at time* $t = 0.5$ *estimated using* $N_0 = 2 \times 10^5$ *realizations of the TRM method for the domain partition* (3.3). (a) *The expected distribution found by* (3.2). (b) *TRM simulation with compartment size* $h = 0.05$ *and* $\Delta t = 0.0004$. (c) *TRM simulation with compartment size* $h = 0.1$ *and* $\Delta t = 0.0016$. (d) *TRM simulation with compartment size* $h = 0.25$ *and* $\Delta t = 0.01$. Ω_C *can be seen in* (b)–(d) *on the right and* Ω_M *to the left of the white solid line. These simulations were done using sampling* (2.15).

At $t = 0.5$ the molecule positions (for each realization) are binned according to their compartment (or in the case of the molecular regime, counted in bins of area h^2) and a plot of these bin copy numbers divided by $N_0 h^2$ is produced to show the approximate probability density that is generated by the TRM. These probability densities are shown for comparison against the exact solution (3.2) in Figure 4(a) for each compartment size h. In order to see the distribution in each of the tangential and perpendicular directions, a strip in each of these directions with a finite width ($\delta = 0.25$) is taken. So that we can compare distributions in each of the x and y directions for different values of h, we plot the sample distributions in these directions given by $\delta^{-1} \int_{0.5}^{0.75} P(x, y, 0.5)\ \mathrm{d}y$ and $\delta^{-1} \int_{0.5}^{0.75} P(x, y, 0.5)\ \mathrm{d}x$, respectively, and compare these to the analytical solution (see Figure 5, (A) and (B), respectively). A graphical description of these strips can be seen in Figure 4 referenced with (A) and (B). The distributions generated using the TRM match well with the expected distribution and appear to be significantly more accurate as h is decreased.

To better visualize the accuracy of the TRM, we define a measure of the error to be the relative discrepancy between the expected number of molecules in Ω_C and the simulated number of molecules in Ω_C.

$$\mathrm{Error}(t) = \frac{C_{TRM}(t)}{N_0} - \iint_{\Omega_C} P(x, y, t)\ \mathrm{d}x\ \mathrm{d}y, \tag{3.4}$$

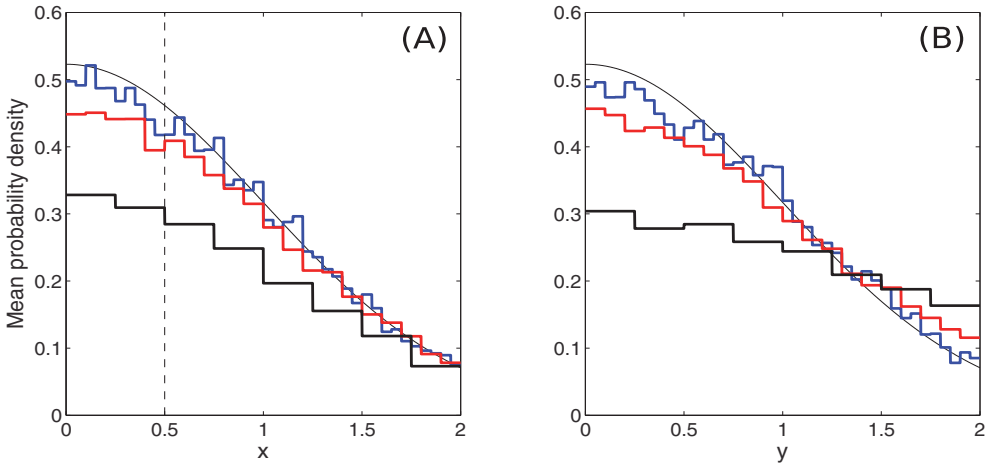

FIG. 5. *Average cross sections of the probability distribution at time* $t = 0.5$ *estimated using* $N_0 = 2 \times 10^5$ *realizations of the TRM method for the domain partition* (3.3) *along strips* (A) *and* (B) *indicated in Figure* 3(a). *The analytic expected distribution found by* (3.2) *is given by the thin black line. TRM simulation estimations are given using* $h = 0.05$ *and* $\Delta t = 0.0004$ *(thick blue line),* $h = 0.1$ *and* $\Delta t = 0.0016$ *(thick red line), and* $h = 0.25$ *and* $\Delta t = 0.01$ *(thick black line). These simulations were done using sampling* (2.15).

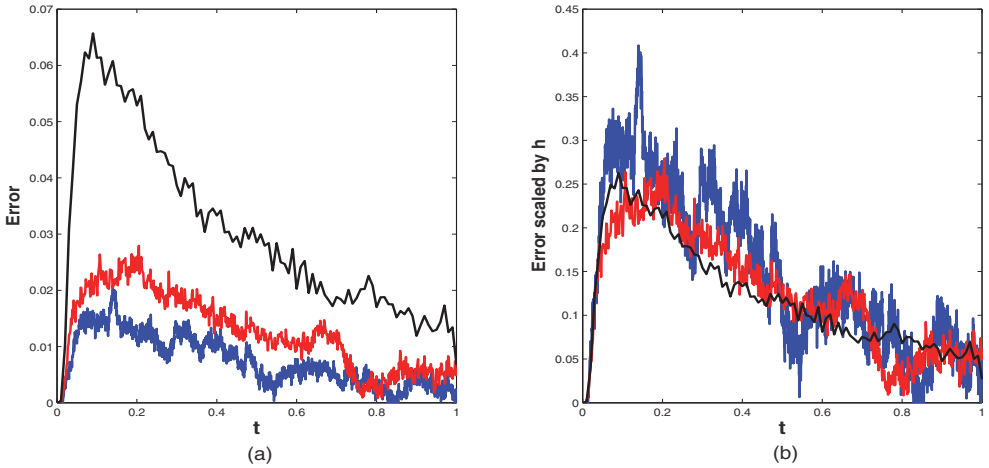

FIG. 6. (a) *The error of the TRM defined by* (3.4) *for* $h = 0.05$ *and* $\Delta t = 0.0004$ *(blue line),* $h = 0.1$ *and* $\Delta t = 0.0016$ *(red line), and* $h = 0.25$ *and* $\Delta t = 0.01$ *(black line). TRM simulations are taken with* $\Omega_C = (0.5, \infty) \times (0, \infty)$ *and* $\Omega_M = (0, 0.5) \times (0, \infty)$. *These simulations were done using sampling* (2.15). *Panel* (b) *results from panel* (a) *scaled by* h.

where $C_{TRM}(t)$ is the number of realizations of the TRM which have the molecule positioned in Ω_C at time t. Therefore, the fraction $C_{TRM}(t)/N_0$ is the approximation of $\iint_{\Omega_C} P(x, y, t)\, \mathrm{d}x\, \mathrm{d}y$ and the error (3.4) measures the accuracy of this approximation.

It is clear from Figure 5, (A), that there is a clear bias of molecules across the interface. This error seems to scale as h. We shall see this is the case in Figure 6.

In Figure 6(a) we present the error (3.4) as a function of time for the $h = 0.05$, $h = 0.1$, and $h = 0.25$ simulations. There is a maximum in this error around $t \sim 0.1$ for all simulations. The predicted error on the boundary (see section 2.1) is proportional

to the net flux over the interface ($h\bar{p}_x/2 + O(h^2)$). We note that this flux reaches a maximum (according to the exact solution (3.2)) at around $t = 1/24$. The reason the maximum of our measured error does not match up with this time is because the error at the interface is described by a small discontinuity in the distribution on the boundary; this discontinuity then diffuses into each of the subdomains. After $t = 1/24$ the discontinuity is reduced, thereby reducing this bias effect, but there is still some time before the distributions are corrected by diffusion. It is for this reason that coupling at the interface correctly is so crucial. A small bias in the flow over the interface in one direction can lead to an avalanching effect on the distribution. While the TRM cannot entirely eliminate the error that is associated with changing of regime, it does optimize the error. We also expect the error, however, to be proportional to h. We can see that this is the case by plotting the error (3.4) divided by h for each simulation (Figure 6(b)). Each of the three curves in Figure 6(b) approximately overlays, implying that the leading order term of the error is $O(h)$. This means that in the continuous limit $h \to 0$ the error that is due to the TRM appoximately converges linearly with h, as expected.

Figure 5 (right panel) demonstrates an unexpected dispersion artifact along the tangential direction to the interface which is amplified by increasing h. This dispersion can also be indirectly seen in the amplitude of the distributions in Figure 5, (A). The purpose of the TRM is to match the concentration and perpendicular flux of molecules at the boundary in the most optimal way given small h and small Δt. In our analysis, we restricted the algorithm parameters to the case $D\Delta t \sim h^2$. In some applications, this might not be a preferred parameter regime because Δt determines the resolution of the microscopic region Ω_M, and if $D\Delta t \sim h^2$, then this resolution is no better than the compartment-based regime. One must be careful in this case since for $D\Delta t \ll h^2$, the parameter $\Phi = 2\Lambda/\sqrt{\pi}$ (defined by (2.11)) may become significantly larger than 1. The mathematical analysis in section 2.1, which assumed $D\Delta t \sim h^2$, had the capability of balancing $O(h)$ terms for the tangential distribution $F(y)$. Previously, terms of the form Φh^2 in (2.9)–(2.10) (which were ignored as "too small," $O(h^2)$) now become as large as terms $O(h)$. This means that the analysis is valid only to leading order, giving a tangential distribution (2.16). If (2.14) is used, then the additional $O(\Phi h^2)$ terms can be seen to manifest into an artificial increase in the dispersion inside the boundary layer near the interface in the tangential direction. This effect can be seen graphically in Figure 7(c).

The increase in the dispersion in the tangential direction may also be explained by following the TRM mechanism. Consider molecules in Ω_M close to the interface between Ω_M and Ω_C. If these molecules are sufficiently close to the interface, they are likely to be absorbed into a compartment in Ω_C. To compensate for this rapid absorption of molecules, the compartments on the interface must return these molecules to the boundary layer at comparable rates. Since, as $\Delta t \to 0$, the boundary layer gets thinner, this increases the rate of resorption of molecules having just come from Ω_C. If a molecule enters an interfacial compartment $\mathcal{C}_{0,j}$ near the boundary to the adjacent compartment $\mathcal{C}_{0,j-1}$, then this molecule effectively jumps a distance $h/2$ in the tangential direction (because its position in Ω_C can be considered as the center of $\mathcal{C}_{0,j}$). This molecule is then rapidly interchanged between Ω_M and $\mathcal{C}_{0,j}$ each time with a new tangential coordinate until the tangential coordinate falls out of line with $\mathcal{C}_j$ or the molecule diffuses away from the interface. The former of these two options occurs more often if Δt is small since the tangential coordinate is rapidly resampled until the 0.25 chance of being sampled outside the compartment $\mathcal{C}_j$ is realized if we use (2.14). In these situations, it is better to use (2.16) for the tangential coordinate.

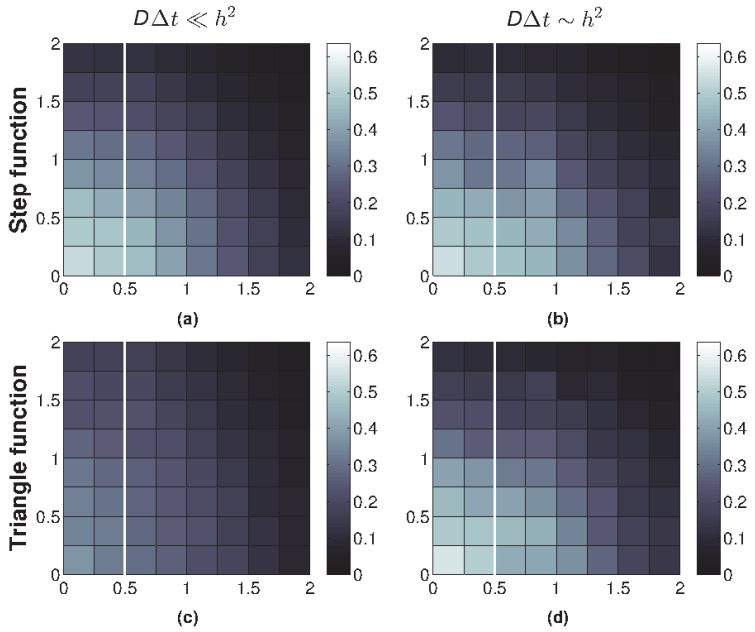

FIG. 7. *Probability distribution at time* $t = 0.5$ *estimated using* $N_0 = 2 \times 10^5$ *realizations of the TRM method for the domain partition* (3.3). *In all simulations* $h = 0.25$ *and* $D = 1$. Ω_C *can be seen in* (a)–(d) *on the right and* Ω_M *to the left of the white solid line denoting interface* I. *TRM simulations with* (a) $D\Delta t = 10^{-5} \ll h^2$ *and* (2.15); (b) $D\Delta t = 0.01 \sim h^2$ *and* (2.15); (c) $D\Delta t = 10^{-5} \ll h^2$ *and* (2.17); *and* (d) $D\Delta t = 0.01 \sim h^2$ *and* (2.17).

This is because (2.16) restricts the molecule initiation to the compartment from which it came. Furthermore, one can reduce this effect by reducing the size of h. Reducing h helps to reduce Φ. While reducing h helps to reduce the error on the boundary, it also increases the computational time. In order to avoid excess computational cost refinement of the lattice is only required near the interface. Furthermore, in a practical sense, there is a limit to which reducing h will help to improve the error of the TRM. This limit occurs in the presence of bimolecular reactions near the interface. Reducing the size of h beyond the small h limit near the interface will result in a reduction of the reaction rate locally.

It is possible to show that this numerical artifact is improved, if h cannot be reduced, by using step function (2.16) instead of triangle function (2.14) to sample molecule positions tangentially to the interface. However, if $D\Delta t \sim h^2$, then (2.14) offers the best results. This is demonstrated in Figure 7. In Figure 7, the least amount of artificial dispersion is achieved if $D\Delta t \sim h^2$ using the triangle function sampling (2.14) but the triangle function sampling introduces more severe artificial dispersion along the interface than step function sampling (2.16) if $D\Delta t \ll h^2$. It is therefore the recommendation of the authors that unless parameters Δt and h can be chosen such that $D\Delta t \sim h^2$, the safest option is to use the step function, which is accurate to leading order under any regime. Alternatively, one could use (4.1) as we shall see later.

3.2. Interface with a corner. To demonstrate that the TRM produces good results when there is a corner in the interface, we present also the results of TRM

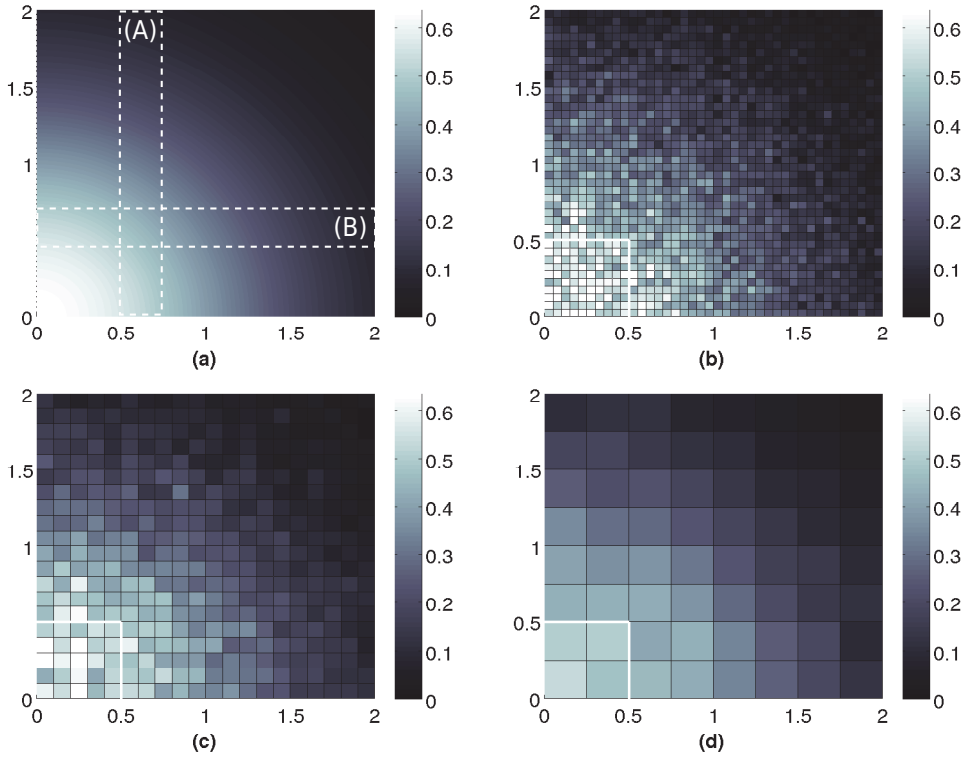

FIG. 8. *Probability distribution at time* $t = 0.5$ *estimated using* $N_0 = 2 \times 10^5$ *realizations of the TRM method for the domain partition* (3.5). (a) *The expected distribution found by the exact solution* (3.2). (b) *TRM simulation with compartment size* $h = 0.05$ *and* $\Delta t = 0.0004$. (c) *TRM simulation with compartment size* $h = 0.1$ *and* $\Delta t = 0.0016$. (d) *TRM simulation with compartment size* $h = 0.25$ *and* $\Delta t = 0.01$. Ω_C *can be seen in* (b)–(d) *outside of* Ω_M *which is boxed by the white solid line (interface* I*) about the origin. These simulations were done using sampling* (2.17)–(2.18) *near the corners according to the approach described in section* 2.2.

simulations of the same problem as in section 3.1 with subdomains redefined as follows:

$$\Omega_M = (0, 0.5) \times (0, 0.5), \qquad \Omega_C = (0, 0.5) \times (0.5, \infty) \cup (0.5, \infty) \times (0, \infty). \tag{3.5}$$

The details of the TRM implementation of corners are discussed in section 2.2. The corner is oriented as in Figure 3(b), i.e., the TRM implementation presented in section 2.2 for the corner orientation in Figure 3(a) is adjusted (by a simple rotation) to the corner orientation in Figure 3(b).

In Figure 8 we present the distributions that result from using the TRM for the domain partition (3.5). These distributions are calculated in the same way as those distributions found in Figure 4. The distributions are plotted, similarly, at $t = 0.5$. There is good agreement with the expected distribution (Figure 8(a)) especially for small h.

Figure 9 shows the distributions in both the x (A) and Y (B) directions, respectively. Bias from high concentration to low concentration over the interface can be seen as expected.

In Figure 10(a), we present the error (3.4) as a function of time for the $h = 0.05$, $h = 0.1$, and $h = 0.25$ simulations. To verify that the error due to the TRM is still

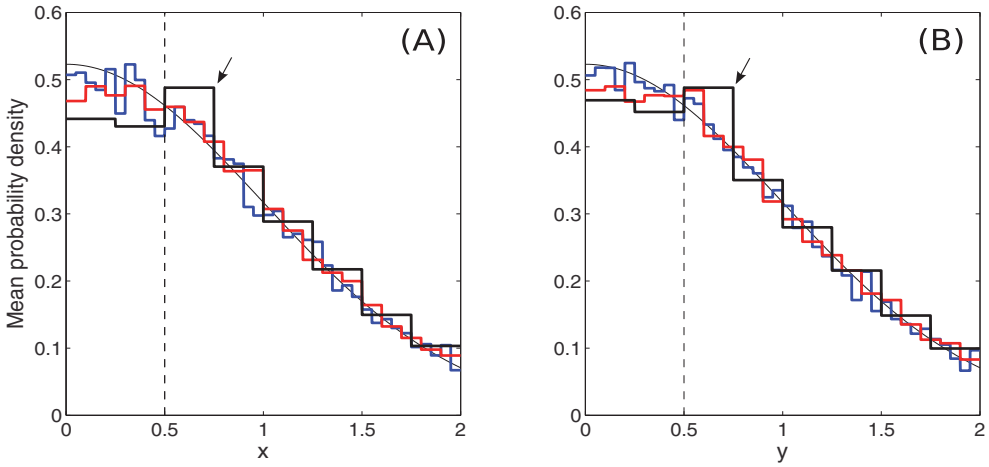

FIG. 9. *Average cross sections of the probability distribution at time* $t = 0.5$ *estimated using* $N_0 = 2 \times 10^5$ *realizations of the TRM method for the domain partition* (3.3) *along strips* (A) *and* (B) *indicated in Figure* 8(a). *The analytic expected distribution found by* (3.2) *is given by the thin black line. TRM simulation estimations are given using* $h = 0.05$ *and* $\Delta t = 0.0004$ *(thick blue line),* $h = 0.1$ *and* $\Delta t = 0.0016$ *(thick red line), and* $h = 0.25$ *and* $\Delta t = 0.01$ *(thick black line). These simulations were done using sampling* (2.17)–(2.18) *near the corners according to the approach described in section* 2.2.

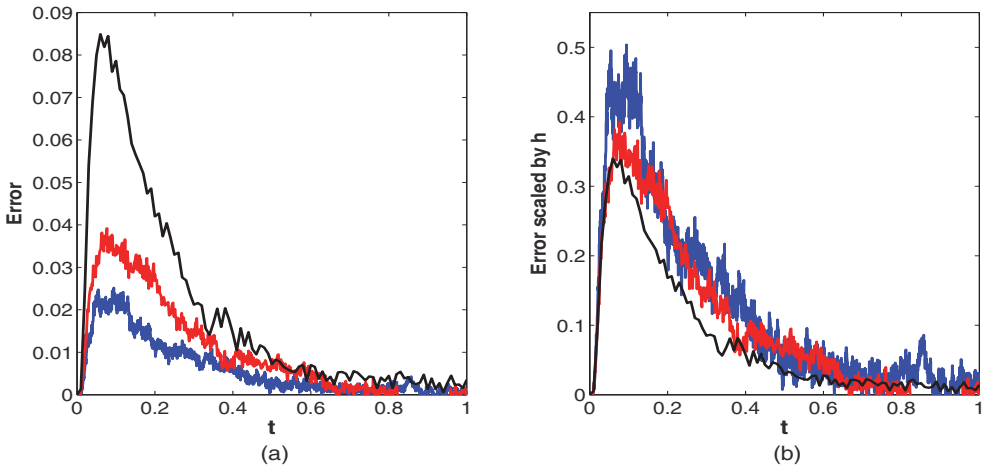

FIG. 10. (a) *The error of the TRM defined by* (3.4) *for* $h = 0.05$ *and* $\Delta t = 0.0004$ *(blue line),* $h = 0.1$ *and* $\Delta t = 0.0016$ *(red line), and* $h = 0.25$ *and* $\Delta t = 0.01$ *(black line). TRM simulations are taken with* Ω_M *and* Ω_C *defined in* (3.5). *Panel* (b) *results from* (a) *scaled by* h.

$O(h)$ when the interface has a corner in it, Figure 10(b) shows the error for the TRM simulations scaled by h.

In Figure 11(a), we again see the artifact for small Δt in the compartment described by the region $x \in [0.5, 0.75)$, $y \in [0.5, 0.75)$: an unexpectedly large number of molecules. This is because diffusion is biased tangentially along both sides of the interface (due to the large h and small Δt as we discussed in section 3.1) and these molecules gather at the corner. This artifact can be seen clearly in Figure 9 (indicated with a small arrow).

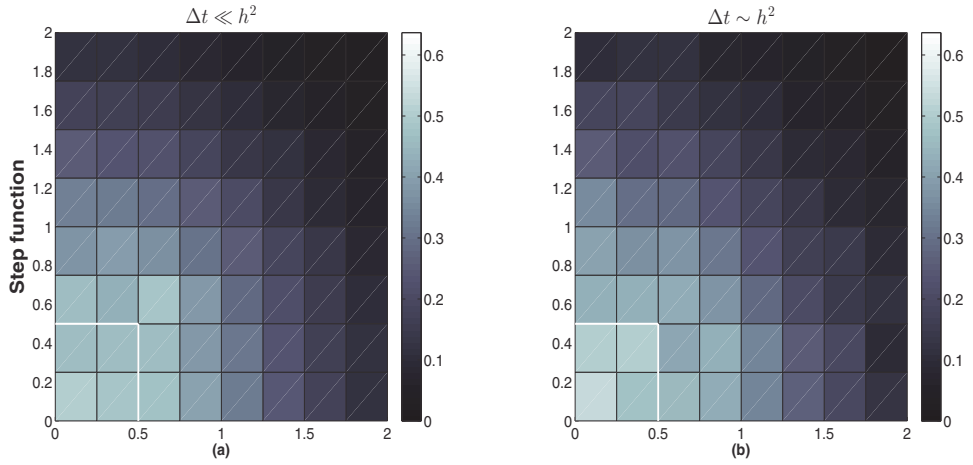

FIG. 11. *Probability distribution at time* $t = 0.5$ *estimated using* $N_0 = 2 \times 10^5$ *realizations of the TRM method for the domain partition* (3.5). *In both simulations* $h = 0.25$ *and* $D = 1$. Ω_C *can be seen outside of* Ω_M *which is boxed by the white solid line denoting interface* I. *TRM simulations with* (a) $D\Delta t = 10^{-5} \ll h^2$, (b) $D\Delta t = 0.01 \sim h^2$. *These simulations were done using sampling* (2.17)–(2.18) *near the corners according to the approach described in section* 2.2.

4. Discussion and conclusions. In this paper we presented an analysis of the TRM on regular lattices in dimensions larger than one. We derived TRM parameters to simulate diffusing molecules migrating over interface I that separates domain Ω_C in which molecules are constrained to a lattice and domain Ω_M whereby molecules can diffuse in continuous space. The TRM algorithm is presented in Figure 1. Our derivation considers the natural diffusion relationship between time scales (resolved with small time steps Δt) and spatial scales (resolved with small lattice spacings h), that is, $D\Delta t \sim h^2$. We were able to show that with these assumptions, in principal, seamless diffusion could be achieved by increasing the resolution of the algorithm parameters h and Δt. This is a problem in applications due to computational limitations and instances involving bimolecular reactions due to the well-known divergent error as $h \to 0$. We found that if $D\Delta t \sim h^2$ are small the error due to the TRM interface is proportional to the net flux of molecules to leading order in h; however, other artifacts are incurred if $D\Delta t \ll h^2$ (which would be common for many applications). We discussed the physical and mathematical source of these artifacts and methods for reducing them.

In high dimensionality, we showed that the parameter $\Phi_{i,j}$ defined in (1.10) is unchanged from the 1D case (1.11). The distribution $f(\mathbf{x})$ for placing molecules in Ω_M was presented in (2.19). In particular, each tangential direction to the interface may be treated independently and in the same way. We presented two different approaches (2.14) and (2.16) for sampling tangential directions.

We performed numerical examples for two cases $D\Delta t \ll h^2$ and $D\Delta t \sim h^2$. In the case $D\Delta t \ll h^2$, the step function approximation (2.16) is the most appropriate choice. In particular, the distribution for placing molecules in Ω_M is given by (2.17) for 2D problems. In the case $D\Delta t \sim h^2$, the triangle function approximation (2.14) is the most appropriate choice, i.e., the distribution for placing molecules in Ω_M is given by (2.15). Moreover, Figure 7 demonstrates that the overall best results (in terms of accuracy) can be obtained in the case $D\Delta t \sim h^2$ and (2.14). However, imposing

the condition $D\Delta t \sim h^2$ over the whole domain Ω_C might lead to computationally intensive simulations. A natural solution to this problem would be to use unstructured meshes [4] where compartments can be of different sizes. Then we could impose the condition $D\Delta t \sim h^2$ for compartments close the interface I (to maximize accuracy) and the condition $D\Delta t \ll h^2$ for compartments further from the interface (to maximize efficiency).

It is unclear at which stage on the interval defined by $0 < D\Delta t < h^2$ one should particularly switch between using the triangle (2.14) or step (2.16) functions. Using a narrow 2D domain, $-1 < x < 1$ and $-\infty < y < \infty$, with an interface at $x = 0$ we were able to simulate 2×10^5 molecules from a starting y-coordinate of $y = 0$ from $t = 0$ to $t = 100$. Measuring the variance in the tangential y-coordinate we could calculate the effective tangential diffusion constant. Varying the time step Δt we found that a switch between using a triangle (2.14) or step function (2.16) for placing molecules tangentially to the interface should occur at around $D\Delta t = \beta h^2$ where $\beta \approx 0.15 \pm 0.05$. One might heuristically explain these functions under their respective conditions ($D\Delta t \sim h^2$ and $D\Delta t \ll h^2$) by considering that molecules in the compartments are uniformly distributed over the compartment. Within the time step t to $t + \Delta t$ this uniform distribution "spreads" outside of the compartment, according to the diffusion equation, in the Ω_M regime. It should also be noted that a molecule that exits the compartment at some point within this time interval does so for an average of a quarter of the time interval $(t, t + \Delta t]$. If this is the case, then the most natural solution for the tangential distribution of leaked molecules should be

$$f(y) = \frac{1}{2h}\left(\operatorname{erf}\left(\frac{2y-h}{\sqrt{2D\Delta t}}\right) - \operatorname{erf}\left(\frac{2y+h}{\sqrt{2D\Delta t}}\right)\right). \tag{4.1}$$

As Δt, $h \to 0$, this equation appears similar to (2.14) when $D\Delta t \sim h^2$ and (2.16) when $D\Delta t \ll h^2$. Thus, adopting (4.1) avoids the user having to "choose" between (2.14) and (2.16). Furthermore, it has been shown from testing to give comparable results to the optimal choice of tangential placement in both regimes.

Given random numbers r_u and r_n sampled from the uniform distribution on the interval $[0, 1]$ and the standard normal distribution, respectively, a sample from the distribution (4.1) is given by $f_{\text{sample}} = (r_u - 0.5)h + \sqrt{D\Delta t/2}r_n$. This function can be used as a substitute for the triangle or step functions and will be accurate for all $D\Delta t \lessapprox h^2$.

An algorithm similar to the TRM was recently published by Klann, Ganguly, and Koeppl [23]. In this algorithm, compartment-based and molecular-based regions are coupled. It is not clear how exactly Klann, Ganguly, and Koeppl [23] couple different regimes. However, several differences between their approach and the TRM can be identified.

The analysis presented in [10] and in section 2 reveals that some steps of the hybrid method in [23] are not optimal. For example, in [23], a molecule migrates from the compartment-based algorithm with a propensity which is natural for the lattice. This means that they have taken a value of $\Phi = 1$ instead of Φ given by (1.11). Instead of placing the molecule with a distribution given by (2.15) into the the molecular-based domain they place the molecule within the compartment that corresponds with a natural extension of the compartment-based approach. Furthermore, molecules are transferred back into compartment-based molecules without condition (b) in section 1.3.2. (This corresponds to a value of $\Psi = 1/2$ instead of Ψ given by (1.11).) It is our experience that somewhat ad hoc or heuristic coupling of this type

between compartment-based and molecular-based regions may lead to heavy biasing of molecules, especially in the case when the expected net flux over the interface is high. The direction and extent of the bias depends on Δt and h and D as well as the natural net flux of molecules over the interface.

Hellander, Hellander, and Lötstedt [20] present a similar approach to [23] for interfacing molecular-based and compartment-based models. Their method allows for transfer of molecules from Ω_C to Ω_M by means of a jump into a compartment region that is outlined in Ω_M as well as Ω_C. The initiation of molecules into Ω_M involves placing the molecules with a uniform distribution over this pseudocompartment. The algorithm then uses GFRD to update molecules in the molecular-based domain. While (as with Klann, Ganguly, and Koeppl) this algorithm may have a significant bias for molecules to travel over the interface depending on the compartment sizes and the time steps that are determined by GFRD, Hellander, Hellander, and Lötstedt also present a method for coupling co-existing molecular- and compartment-based regimes in which some molecules exist off-lattice and others exist on an overlapping lattice. Such a coupling technique could be used to overcome the bias by introducing an overlap region between the two regimes. A similar approach is used by Franz et al. to improve the accuracy of coupling deterministic PDEs with microscopic molecular-based simulations [13].

Unlike [23] and [20] the TRM has not yet been adapted to irregular compartments or to a dynamic interface moving in response to shifting molecular concentrations. These adaptations should be possible and would improve the applicability of the TRM to modeling problems in biology.

REFERENCES

[1] F. Alexander, A. Garcia, and D. Tartakovsky, *Algorithm refinement for stochastic partial differential equations:* I. *Linear diffusion*, J. Comput. Phys., 182 (2002), pp. 47–66.

[2] M. Ander, P. Beltrao, B. Di Ventura, J. Ferkinghoff-Borg, M. Foglierini, A. Kaplan, C. Lemerle, I. Tomás-Oliveira, and L. Serrano, *SmartCell, a framework to simulate cellular processes that combines stochastic approximation with diffusion and localisation: Analysis of simple networks*, Systems Biol., 1 (2004), pp. 129–138.

[3] S. Andrews and D. Bray, *Stochastic simulation of chemical reactions with spatial resolution and single molecule detail*, Phys. Biol., 1 (2004), pp. 137–151.

[4] S. Engblom, L. Ferm, A. Hellander, and P. Lötstedt, *Simulation of stochastic reaction-diffusion processes on unstructured meshes*, SIAM J. Sci. Comput., 31 (2009), pp. 1774–1797.

[5] R. Erban and S. J. Chapman, *Reactive boundary conditions for stochastic simulations of reaction-diffusion processes*, Phys. Biol., 4 (2007), pp. 16–28.

[6] R. Erban and S. J. Chapman, *Stochastic modelling of reaction-diffusion processes: Algorithms for bimolecular reactions*, Phys. Biol., 6 (2009), p. 046001.

[7] R. Erban, S. J. Chapman, and P. Maini, *A Practical Guide to Stochastic Simulations of Reaction-Diffusion Processes*, arXiv:0704.1908, 2007.

[8] R. Erban, M. Flegg, and G. Papoian, *Multiscale stochastic reaction-diffusion modelling: application to actin dynamics in filopodia*, Bull. Math. Biol., 76 (2014), pp. 799–818.

[9] L. Ferm, A. Hellander, and P. Lötstedt, *An adaptive algorithm for simulation of stochastic reaction-diffusion processes*, J. Comput. Phys., 229 (2010), pp. 343–360.

[10] M. Flegg, J. Chapman, and R. Erban, *The two-regime method for optimizing stochastic reaction-diffusion simulations*, J. Roy. Soc. Interface, 9 (2012), pp. 859–868.

[11] M. Flegg, S. Rüdiger, and R. Erban, *Diffusive spatio-temporal noise in a first-passage time model for intracellular calcium release*, J. Chem. Phys., 138 (2013), 154103.

[12] E. Flekkøy, J. Feder, and G. Wagner, *Coupling particles and fields in a diffusive hybrid model*, Phys. Rev. E, 64 (2001), 066302.

[13] B. Franz, M. Flegg, J. Chapman, and R. Erban, *Multiscale reaction-diffusion algorithms: PDE-assisted Brownian dynamics*, SIAM J. Appl. Math., 73 (2013), pp. 1224–1247.

[14] T. Geyer, C. Gorba, and V. Helms, *Interfacing Brownian dynamics simulations*, J. Chem. Phys., 120 (2004), pp. 4573–4580.
[15] M. Gibson and J. Bruck, *Efficient exact stochastic simulation of chemical systems with many species and many channels*, J. Phys. Chem. A, 104 (2000), pp. 1876–1889.
[16] D. Gillespie, *Exact stochastic simulation of coupled chemical reactions*, J. Phys. Chem., 81 (1977), pp. 2340–2361.
[17] D. Gillespie, *Approximate accelerated stochastic simulation of chemically reacting systems*, J. Chem. Phys., 115 (2001), pp. 1716–1733.
[18] C. Gorba, T. Geyer, and V. Helms, *Brownian dynamics simulations of simplified cytochrome c molecules in the presence of a charged surface*, J. Chem. Phys., 121 (2004), pp. 457–464.
[19] J. Hattne, D. Fange, and J. Elf, *Stochastic reaction-diffusion simulation with MesoRD*, Bioinformatics, 21 (2005), pp. 2923–2924.
[20] A. Hellander, S. Hellander, and P. Lötstedt, *Coupled mesoscopic and microscopic simulation of stochastic reaction-diffusion processes in mixed dimensions*, Multiscale Model. Simul., 10 (2012), pp. 585–611.
[21] S. Isaacson, *A convergent reaction-diffusion master equation*, J. Chem. Phys., 139 (2013), 054101.
[22] S. Khokhlova and N. Agmon, *Green's function for reversible geminate reaction with volume reactivity*, J. Chem. Phys., 137 (2012), 184103.
[23] M. Klann, A. Ganguly, and H. Koeppl, *Hybrid spatial Gillespie and particle tracking simulation*, Bioinformatics, 28 (2012), pp. i549–i555.
[24] J. Lipková, K. Zygalakis, J. Chapman, and R. Erban, *Analysis of Brownian dynamics simulations of reversible bimolecular reactions*, SIAM J. Appl. Math., 71 (2011), pp. 714–730.
[25] K. Lipkow, S. Andrews, and D. Bray, *Simulated diffusion of phosphorylated CheY through the cytoplasm of Escherichia coli*, J. Bacteriol., 187 (2005), pp. 45–53.
[26] E. Moro, *Hybrid method for simulating front propagation in reaction-diffusion systems*, Phys. Rev. E, 69 (2004), 060101.
[27] S. Andrews and D. Bray, *First-passage kinetic monte carlo method*, Phys. Rev. E, 80 (2009), 066701.
[28] J. Stiles and T. Bartol, *Monte Carlo methods for simulating realistic synaptic microphysiology using MCell*, in Computational Neuroscience: Realistic Modeling for Experimentalists, E. Schutter, ed., CRC Press, Boca Raton, FL, 2001, pp. 87–127.
[29] K. Takahashi, S. Tanase-Nicola, and P. ten Wolde, *Spatio-temporal correlations can drastically change the response of a mapk pathway*, Proc. Natl. Acad. Sci. USA, 107 (2010), pp. 19820–19825.
[30] W. van Gunsteren and H. Berendsen, *Algorithms for Brownian dynamics*, Molecular Phys., 45 (1982), pp. 637–647.
[31] N. van Kampen, *Stochastic Processes in Physics and Chemistry,* 3rd ed., North-Holland, Amsterdam, 2007.
[32] J. van Zon and P. ten Wolde, *Green's-function reaction dynamics: A particle-based approach for simulating biochemical networks in time and space*, J. Chem. Phys., 123 (2005), 234910.
[33] G. Wagner and E. Flekkøy, *Hybrid computations with flux exchange*, Philos. Trans. R. Soc. London Ser. A Math. Phys. Eng. Sci., 362 (2004), pp. 1655–1665.
[34] S. Wils and E. De Schutter, *STEPS: Modeling and simulating complex reaction-diffusion systems with Python*, Front. Neuroinformatics, 3 (2009), pp. 1–8.